Feedforward information and zero-lag synchronization in the sensory thalamo-cortical circuit are modulated during stimulus perception

Adrià Tauste Campo[1,2,*], Yuriria Vázquez[3,4], Manuel Álvarez[3], Antonio Zainos[3], Román Rossi-Pool[3], Gustavo Deco[2,5], and Ranulfo Romo[3,6,*]

[1]BBRC, C/ Wellington, 30, 08005 Barcelona, Spain, ORCID=0000-0003-0982-4017

[2]Center for Brain and Cognition, Department of Information and Communication Technologies, Universitat Pompeu Fabra, 08003 Barcelona, Spain

[3]Instituto de Fisiología Celular–Neurociencias, Universidad Nacional Autónoma de México, 04510 Mexico City, Mexico

[4]The Rockefeller University, 1230 York Avenue, New York, NY 10065, USA

[5]Institució Catalana de Recerca i Estudis Avançats, Passeig Lluís Companys, 23, 08010 Barcelona, Spain

[6]El Colegio Nacional, 06020 Mexico City, Mexico

*Correspondence: rromo@ifc.unam.mx, adria.tauste@gmail.com

Post-print version of the article:

Tauste Campo et al (2019). Feed-forward information and zero-lag synchronization in the sensory thalamocortical circuit are modulated during stimulus perception. Proceedings of the National Academy of Sciences, 116(15), 7513-7522.

https://doi.org/10.1073/pnas.1819095116

ABSTRACT

The direction of functional information flow in the sensory thalamo-cortical circuit may play a role in stimulus perception, but, surprisingly, this process is poorly understood. We addressed this problem by evaluating a directional information measure between simultaneously recorded neurons from somatosensory thalamus (VPL) and somatosensory cortex (S1) sharing the same cutaneous receptive field, while monkeys judged the presence or absence of a tactile stimulus. During stimulus presence, feedforward information (VPL→S1) increased as a function of the stimulus amplitude, while pure feedback information (S1→VPL) was unaffected. In parallel, zero-lag interaction emerged with increasing stimulus amplitude, reflecting externally-driven thalamo-cortical synchronization during stimulus processing. Furthermore, VPL→S1 information decreased during error trials. Also, VPL→S1 and zero-lag interaction decreased when monkeys were not required to report the stimulus presence. These findings provide evidence that both the direction of information flow and the instant synchronization in the sensory thalamo-cortical circuit play a role in stimulus perception.

KEYWORDS

Behaving Monkeys; Somatosensory Thalamo-Cortical Circuit; Tactile Detection Task; Simultaneous Single-Unit Recordings; Directed Information-Theoretic Measure;

SIGNIFICANCE STATEMENT

The direction of functional information flow between brain circuits may be key in cognitive functions. We addressed this problem by evaluating a directional correlation measure between simultaneously recorded neurons from somatosensory thalamus (VPL) and somatosensory cortex (S1) sharing the same cutaneous receptive field, while monkeys judged the presence or absence of a tactile stimulus. During stimulus presence, feedforward (VPL→S1) information increased as function of the stimulus amplitude, while feedback (S1→VPL) information was unaffected. Simultaneously, zero-lag interaction emerged with increasing stimulus amplitude, contributing to thalamo-cortical synchronization. Furthermore, VPL→S1 information decreased during error trials. Also, both VPL→S1 and zero-lag interactions decreased when monkeys were not required to report stimulus presence. Thus, directional and coordinated information in the thalamo-cortical circuit are associated with stimulus perception.

Author contributions: A.T.C., Y.V., M.A., A.Z., R.R.-P., G.D., and R.R. contributed to different aspects of the study, including design and performance of research and data analysis. A.T.C., R.R.-P., G.D. and R.R. wrote the paper. A.T.C. and R.R. supervised all stages of the study.

INTRODUCTION

A major challenge in systems neuroscience involves understanding how perceptual experiences arise from coordinated neural activity, and how functional information flows among the interacting neurons (1-5). The sensory thalamus is an essential node within the perceptual circuit, relaying stimulus information from the periphery to cortex (6). Given the connectivity between the thalamus and cortex, feedback cortico-thalamic inputs could modulate feedforward thalamo-cortical stimulus information transmission during perception (7-10). Thus, the thalamus could act as a processing unit in continuous interaction with the cortex (6,11,12). Evidence supporting this view relies from previous studies in anesthetized (13-15) and awake animals (10,16). However, it is unclear how feedforward and feedback information flows coexist within the thalamo-cortical circuit and whether they correlate with the subject's perception.

To address these questions, we recorded the simultaneous activity of single neurons in the ventral posterolateral nucleus (VPL) of the somatosensory thalamus and in primary somatosensory cortex (S1) sharing the same cutaneous receptive field, while monkeys performed a vibrotactile detection task. The animals were trained to report the presence or absence of a tactile stimulus of variable amplitude. In this task, previous works showed that VPL and S1 neurons encode mostly the physical features of the stimulus (17,18). These findings rise several questions. First, how sensory information is communicated between the VPL and S1 at the level of single neurons? Second, what is the balance between the information flowing in a feedforward direction (VPL→S1) and in a feedback (S1→VPL) direction? Third, does the information flow between VPL and S1 correlate with the subject's perception?

In the current work, we addressed the above questions by detecting time-varying directional couplings between the recorded VPL and S1 neuron pairs across many trials as a measure of the functional thalamo-cortical information flow needed to

perform a vibrotactile detection task. During the stimulus presence, feedforward (VPL→S1) information largely prevailed over feedback (S1→VPL) information. Interestingly, zero-lag interactions emerged with the stimulus amplitude above detection threshold, suggesting the existence of cortical common inputs facilitating the transmission of stimulus information. Critically, at the stimulus onset, feedforward information correlated with the subject's perception. During a variant of the detection task (passive condition, in which no response was required from the animal), feedforward information was reduced during the expected stimulation windows of s stimulus-present and stimulus-absent trials, while zero-lag interaction was mainly reduced in the first half of the stimulus. Taken together, our results characterize the functional information flow between VPL-S1 neuron pairs during tactile perception. They reveal that feedforward information besides relaying stimulus information, conveys task-context information, whereas zero-lag interactions might reflect the cortically-driven coordinated activity of VPL and S1 that is required for information transmission during task performance.

RESULTS

Two monkeys *(Macaca Mulatta)* were trained to perform a tactile detection task (2,3). In each trial, the animal had to report whether the tip of a mechanical stimulator vibrated or not (Fig. 1A). Stimuli were sinusoidal, had a fixed frequency of 20 Hz and were delivered to the glabrous skin of one fingertip; crucially, they varied in amplitude across trials. Stimulus-present trials were interleaved with an equal number of stimulus-absent trials in which no mechanical vibrations were delivered (Fig. 1A). The presence or absence of the stimulus (0.5 s) was preceded by a variable pre-stimulus period (1.5–3 s), followed by a fixed post-stimulus delay period of 3 s before the monkey reported its decision by pressing one of two push-buttons (Fig. 1A). Stimulus detection thresholds were calculated from the behavioral responses (left panel of Fig. 1B). Importantly, depending on the monkeys' responses, trials could be classified into four types: hits and misses in the stimulus-present trials, and correct rejections and false alarms in the stimulus-absent condition (right panel of

Fig. 1B). Once the animals performed the task at near detection threshold (8 µm), we recorded the simultaneous activity of spike trains from individual neurons from VPL and S1 (areas 3b or 1, Fig. 1C), while monkeys performed the task. Here, it is important to highlight that the recorded neuron pairs (n = 84) from the VPL and S1 shared exactly the same cutaneous receptive fields (Fig. 1D). Fig. 1E shows that the neurons of VPL and S1 modulate their firing rate during the stimulus-present condition (left panel), but not during the stimulus-absent condition (right panel). Thus, it appears an optimal experimental condition for assessing the time-varying functional information flow between neuron pairs from VPL and S1 during the detection task.

Assessing directional information flow between VPL and S1

It is well established that the VPL relays information from the skin mechanoreceptors up to S1 (Fig. 1C and 1D). This knowledge allows us to test the following hypothesis in the detection task: after the stimulus onset the flow of functional information becomes crucially larger in the VPL→S1 direction than in the S1→VPL direction. However, given the stronger anatomical connectivity from S1 to VPL than from VPL to S1 (12), the second hypothesis is that the flow of functional information is higher from S1→VPL than from VPL→S1. Importantly, we also hypothesize that the information flow between VPL and S1 could be affected by task conditions (Fig. 1B). We addressed all these hypotheses by using a non-parametric method that measures directional information flows between the simultaneously recorded spike trains of pairs of VPL-S1 neurons in single trials and within slicing time windows of 0.25ms using a directed information-theoretic measure (5,19,20) (SI Appendix). The method is illustrated in Fig. 2A. To measure single-neuron interactions on a fine temporal scale along each task trial, we estimated delayed versions of the directed information-theoretic measure (SI Appendix, Eq. S1) in both directions (VPL→S1 and S1→VPL) for every pair of simultaneous VPL-S1 spike trains at the short time delays [0,2,4,…,20 ms] (Fig. 2A, left panel). To infer the significance of each estimation, we defined a maximizing-delay statistic (SI Appendix, Eq. S2) and built the corresponding null distribution using circular shifts of the target spike-train sequences (Y^T), which preserved the firing rate and the short-range (0-50ms)

autocorrelation of both spike trains while destroying their temporal alignment (middle panel of Fig. 2A). For each directional spike-train pair, (X^T, Y^T), the method assessed the significance of the statistic together with an unbiased estimation of the statistic value and the maximizing-delay (Fig. 2A, right panel). Directional spike-train pairs associated with significant estimators ($\alpha = 0.05$) will be next referred as Directional Information (*DI*) trials (SI Appendix) and will be represented for different experimental conditions as a percentage over the corresponding pairs and trials.

A first characterization of the VPL-S1 simultaneous activity was done by measuring the percentage of *DI* (SI Appendix, Fig. S1A), as well as the mean *DI* value (SI Appendix, Fig. S1B) for VPL→S1 and S1→VPL directions during the time course of the detection task for spike trains above a firing rate threshold (35Hz). Both quantities were calculated separately for the stimulus-present (left) and stimulus-absent (right) trials. For the analysis of stimulus-present trials here and in the subsequent figures, we removed the variable-time pre-stimulus period in every trial and aligned all trials to the stimulus onset time. The analysis showed that for the stimulus-present trials, the amount of VPL→S1 *DI* (trials = 3216 in neuron pairs = 84, $P < 0.01$, $H > 0.5$, cyan line; SI Appendix, Fig. S1A left) was significantly larger than the amount of S1→VPL *DI* during the first half (250 ms) of the stimulus period and weaker, but still significant during the second half ($H < 0.5$). On the other hand, the strongest effect at stimulus onset was not mimicked by the mean *DI* value ($P < 0.01$, $D < 0.3$; SI Appendix, Fig. S1B left). In contrast, for stimulus-absent trials, the greatest differences were manifested by the amount of *DI* (trials = 4371 in neuron pairs = 84, $P < 0.01$, $H > 0.3$; SI Appendix, Fig. S1A right) during the possible window of stimulation (PWS) with no matching evidence from the mean *DI* value (SI Appendix, Fig. S1B right). Despite its moderate statistical effect ($H<0.5$), Fig. S1 (SI Appendix) shows a positive gap between VPL→S1 and S1→VPL directions already during the pre-stimulus period, which could reflect an underlying directionality imbalance facilitating subsequent sensory information transmission. In conclusion, we restricted our analysis to the percentage of *DI* (rather than the *DI*

mean value) due to its greater sensitivity to detect directionality differences during the stimulus period.

As a first approach, we considered exclusively two directionality cases: VPL→S1 and S1→VPL (SI Appendix, Fig. S1). Yet, when studying *DI* flow for two simultaneous spike T-length trains X^T and Y^T at a given time interval (e.g., 250 ms) one may instead consider three disjoint cases: the spike trains are coupled in only one direction ($X^T \rightarrow Y^T$), in only the opposite direction ($Y^T \rightarrow X^T$) or simultaneously coupled in both directions ($X^T \leftrightarrow Y^T$). In principle, these three cases correspond to neurons in each pair taking three different roles: driver, target or both, which may be associated with distinct functional mechanisms (24). According to this notion, we classified *DI* estimates by pairing the location and role of each neuron per trial. In short, we defined as feedforward information (VPL→ S1) those *DI* estimates involving pairs where the neuron of VPL was only driver and the neuron of S1 was only target. Similarly, we defined as feedback information (S1→VPL) where the neuron of S1 was only driver and the VPL neuron was only target. Finally, pairs where the neuron in VPL and the neuron in S1 were simultaneously drivers and targets (at possible different delays) of that interaction were labeled as bidirectional information. Fig. 2B shows a schematic representation for the three types of *DI* and Fig. 2C-E shows four example pairs of neurons (five repetitive trials; green color for VPL raster plots and cyan color for S1 raster plots) responding during the first 250 ms after stimulus onset holding feedforward (Fig. 2C), feedback (Fig. 2D) and bidirectional (Fig. 2E) information, together with neuron pairs with non-significant *DI* (Fig. 2F). Since the significance analysis leading to *DI* is always single-trial, the choice of five trials in Fig. 2D is only for illustrative purposes here.

Stimulus-presence modulates feedforward and bidirectional information

Having set the above definitions, we first examined for each type of *DI* the average *DI* delay as a putative intrinsic property of each directionality case (SI Appendix, Fig. S2). Bidirectional information occurred at shorter delays than unidirectional information for both stimulus-present (trials = 3217 in neuron pairs = 84, $\langle D = 0.35 \rangle$, time-average Cohen's *d*; SI Appendix, Fig. S2A left) and stimulus-

absent trials (trials = 4731 in neuron pairs = 84, $\langle D = 0.37 \rangle$, time-average Cohen's *d*; SI Appendix, Fig. S2A right). The delay histograms (SI Appendix, Fig. S2B top) outside the stimulus period or the PWS revealed that these differences were, in general, due to higher percentage of zero-delay couplings (around 33%) in bidirectional information as compared with unidirectional information (around 15%). Further, we examined the *DI* delay distribution during the stimulus period (SI Appendix, Fig. S2B). We found that the arrival of the stimulus increased the relative amount of bidirectional information at zero delay (from 33% to 49%). However, the relative amount of feed-forward (from 9 to 19%) and feed-back information (from 9 to 15%) was enhanced at 8ms.

Second, we investigated two main questions regarding feedforward, feedback and bidirectional information: 1) what was the contribution of each *DI* type to a greater amount of VPL→S1 *DI* observed during the stimulus presence? 2) What was the contribution of each neuron pair to this effect? Fig. 3A depicts the percentages of *DI* according to their types (feedforward, feedback, and bidirectional) for stimulus-present (left) and stimulus-absent trials (right) during the time-course of the task. The proposed decomposition highlighted the contribution of each type into the directionality differences illustrated in Fig. S1 (SI Appendix). The increment in the VPL→S1 *DI*, especially after the stimulus onset, was mainly contributed by feedforward information (trials = 3216 in neuron pairs = 84, $P < 0.05$, $H = 0.23$; blue trace in left panel of Fig. 3A) and lesser by the bidirectional information (trials = 3216, neuron pairs = 84, $P < 0.05$, $H = 0.1$; orange trace in left panel of Fig. 3A). In contrast, the increase in the S1→VPL direction (SI Appendix, Fig. S1) could only be explained by an increase in bidirectional information. Indeed, genuine feedback information was not significantly modulated during the stimulus presence ($P > 0.05$; red trace in left panel of Fig. 3A). On the other hand, for stimulus-absent trials, none *DI* type showed a significant modulation (trials = 4271 in neuron pairs = 84, $P > 0.05$; right panel of Fig. 3A).

We then investigated the contribution of each neuron pair to the increment in feedforward and bidirectional information during the first half of the stimulus period in the stimulus-present trials. To do so, we repeated the analysis of Fig. 3A for every

VPL-S1 pair and obtained a stimulus-driven effect size per pair. Fig. 3B illustrates these results by sorting the neuron pairs independently for each *DI* type in a descending effect size order. Consistent with our previous findings, there were more neuron pairs exhibiting large stimulus effects in feedforward and bidirectional information than in feedback information. Besides that, approximately 40% (33/84) and 20% (18/84) of the neuron pairs increased the number of feedforward and bidirectional information, respectively, with moderate and large effect sizes ($H > 0.3$, Fig. 3B).

Next, we asked how often a VPL-S1 neuron pair could simultaneously handle both *DI* modulations during the stimulus period. To address this question, we correlated the stimulus effect sizes associated with each *DI* type across all the recorded VPL-S1 neuron pairs. The correlation value between the effect sizes was rather low ($\rho = -0.11$, $P > 0.5$, Spearman's rho), suggesting that feedforward and bidirectional VPL-S1 information might be modulated by a different thalamo-cortical mechanism. We also analyzed how neuron pairs were differently modulated during stimulus-absent trials (SI Appendix, Fig. S3). To this end, we compared the percentage of feedforward, feedback and bidirectional information per neuron pair during the first interval of the stimulus window and during the first interval of the PWS. Each point in Fig. S3 (SI Appendix) represents a VPL-S1 neuron pair and the histogram of all points' angles with respect to the stimulus-present axis (x-axis: stimulus present, y-axis: stimulus absent) are shown as insets. Therefore, angular values smaller than 45° indicated stronger amount of *DI* during the stimulus period. Thus, mean angular values indicated that the stimulus-present effect ($\theta < 45°$) was more prominently manifested in feedforward ($\theta = 30.5°$; SI Appendix, Fig. S3) and bidirectional information ($\theta = 25.2°$; SI Appendix, Fig. S3) than in feedback information ($\theta = 41.1°$; SI Appendix, Fig. S3). In sum, we provided consistent evidences from independent analyses that tactile stimuli mainly modulated feedforward and bidirectional information in the VPL-S1 neuron pairs.

Correlation between the firing rate and the type of directional information

The statistical method used in this study infers *DI* measurements by preserving the firing rate of both sequences in the null distribution, thus avoiding to a larger extent the bias introduced by fluctuations of the neuronal spikes (25,26). To empirically corroborate this fact, we examined the influence of the firing rate into the observed VPL-S1 *DI*. In previous related works (17,18), we showed that the average firing rate was larger in VPL than in S1 neurons (Fig. 1E). Therefore, the reported increase of feedforward information (as compared to feedback) occurred while the VPL and S1 neurons exhibited similar firing rates. This initially suggested a low dependence between the firing rate and the existence of *DI*. We then tested this hypothesis by correlating the firing rate of driver and target neurons with the existence of incoming/outgoing *DI* (SI Appendix). The obtained Spearman correlation coefficients were significant, but rather low for both driver (intervals = 206360 in neuron pairs = 84, $\rho = 0.11$, $P < 0.05$; SI Appendix, Fig. S4A) and target neurons (intervals = 206360 in neuron pairs = 84, $\rho = 0.07$, $P < 0.05$; SI Appendix, Fig. S4A). Moreover, these results were stable during stimulus-absent trials (intervals = 206280 in neuron pairs = 84, $\rho = 0.1$ for driver spike trains, $\rho = 0.07$ for target spike trains, $P < 0.05$; SI Appendix, Fig. S4B). This shows that the increase in the number of *DI* estimates during the stimulus period could not be merely explained by an increase in the mean firing rate of either the VPL or S1 neurons.

The results shown above suggested that the firing rate might be poorly correlated with the distinct *DI* types. To specifically address this question, we first computed the time-varying correlation (Spearman's rho) between the firing rate in VPL and S1 neurons (SI Appendix, Fig. S4C and D) associated with feedforward, feedback and bidirectional information for stimulus-present (trials = 3216 in neuron pairs = 84; left) and stimulus-absent (trials = 4371 in neuron pairs = 84; right). The results show that the correlation values obtained during the entire time course of the task were upper-bounded by 0.1 for VPL neurons and by 0.2 for S1 neurons. For S1 neurons specifically, the correlation values decreased during the stimulus period. This implies that, for a substantial number of S1 neurons, the reported increase in firing rate (Fig 1E) during the stimulus presence was not accompanied by an increase of

incoming/outgoing *DI* with VPL. Besides, during the stimulus presence, the correlation values were larger for bidirectional than for unidirectional information in VPL and S1 neurons suggesting that neurons holding bidirectional information were likely to manifest larger firing rates in that period. To further study this question, we examined the firing rate of VPL and S1 neurons associated with feedforward, feedback and bidirectional information (Fig. 4, SI Appendix). Our analysis revealed that the firing rate of VPL and S1 neurons was not significantly different ($n = 53$ and $n = 75$, respectively, Wilcoxon rank-sum test, $P > 0.05$; Fig. 4) between feedforward and feedback information across all task intervals, including those from the stimulation period. In contrast, neurons holding bidirectional information showed a significant increase in their firing rate with respect to the unidirectional case during the first interval of the stimulus period ($P < 0.05$; Fig. 4), in agreement with the reported larger correlation observed in the bidirectional type (Fig S4C and D). These increases were manifested at supra-threshold stimulus amplitudes for VPL neurons ($n = 53$, $P < 0.001$; Fig. 4) during the entire stimulus period, while for S1 neurons ($n = 75$, $P < 0.05$; Fig. 4) only during the first interval of the stimulation period. Interestingly, for stimulus-absent trials, bidirectional neurons showed enhanced firing rates during PWS intervals as compared to unidirectional neurons. In sum, these results show that firing rates were not able to discriminate between unidirectional information (feedforward vs. feedback) but could be significantly higher for bidirectional information during specific task intervals beyond the stimulus presence.

Finally, we simulated a stochastic model to evaluate the performance of the *DI* estimation method as a function of the neuronal firing rate and assess any potential bias in the reported empirical correlations with the firing rate (SI Appendix, Fig. S5; details provided in the Legend). The results of the model for parameter values that approximated the average firing rate of neurons and the percentage of *DI* measured in the real data, validated that the spurious correlations introduced by the *DI* estimation method were very low for both unidirectional and bidirectional models (Spearman's $rho<0.08$). In the meantime, the *DI* estimation method was shown to attain large sensitivity values (>90%) even for low firing rates (~35Hz).

The amount of VPL-S1 directional information is modulated by the stimulus amplitude

We showed above that both feedforward and bidirectional VPL-S1 information was enhanced by the stimulus presence, while feedback information was minimally affected (Fig. 3). Furthermore, each *DI* type could be modulated by different neuronal populations. This prompted us to hypothesize that feedforward and bidirectional information could be differently related to the stimulus amplitude. To further investigate this question, we divided the stimulus-present trials into 3 groups based on the stimulus amplitude. We grouped the 9 µm trials within the near-threshold (middle left panel of Fig. 5A) group and defined the supra-threshold (left most panel of Fig. 5A) and sub-threshold (middle right panel of Fig. 5A) groups as those stimulus-present trials above and below 9 µm, respectively. We choose 9 µm as the cut-off amplitude since it is the closer amplitude to the monkey's mean detection threshold (8 µm; Fig. 1B). We also considered stimulus-absent trials for comparison (right most panel of Fig. 5A). First, we quantified the amount of *DI* within each group (Fig. 5A). Notably, we found that the stimulus effect observed for all amplitudes (Fig. 3B) was mainly due to the supra-threshold group (> 9µm). At these amplitudes, feedforward and bidirectional information showed a significant incremental effect (trials = 2237 in neuron pairs = 84, $P < 0.01$, $H = 0.26$ and $H = 0.14$; left most panel of Fig. 5A), while feedback information was not significantly altered ($P > 0.05$). In contrast, for the near-threshold group, the feedforward increment was preserved (trials = 443 in neuron pairs = 84, $P < 0.01$, $H = 0.2$; middle panel of Fig. 5A), while bidirectional information dropped to the prestimulus level ($P > 0.05$). Finally, the sub-threshold amplitudes only showed a weaker significant increase in the amount of feedforward information (trials = 536 in neuron pairs = 84, $P < 0.01$, $H = 0.13$; right panel Fig. 5A). Thus, the results illustrated in Fig. 5A demonstrated that the amount of *DI* was amplitude dependent. To examine this dependency, we focused on the first 250 ms of the stimulus-present period and plotted the percentage of *DI* types as a function of the stimulus amplitude (Fig. 5B). Besides, we computed single-trial (r) and average-trial (R) Spearman's rho correlations between the amount of *DI* and amplitude values (SI Appendix). During

the first 250 ms the amount of each *DI* type was correlated with the stimulus amplitude values as measured by single-trial types ($P < 0.05$; Fig. 5B). But, when considering average-trial correlations, the significance analysis provided different outcomes across *DI* types. Indeed, Fig. 5B shows that feedforward (trials = 7587, r = 0.12 in neuron pairs = 84, R=0.96, $P < 0.01$; left panel of Fig. 5B) and bidirectional (trials = 7587, r = 0.07 in neuron pairs = 84, R=0.87, $P < 0.05$; right panel of Fig. 5B) information exhibited a significant monotonic modulation, while feedback information remained approximately constant over the amplitude values (trials = 7587, r = 0.03 in neuron pairs = 84 , R=0.26, $P > 0.05$; middle panel of Fig. 5B). These effects were further illustrated in Fig. S6 (SI Appendix) by representing feedback and bidirectional against feedforward information, which suggested that the bidirectional trend was mainly driven by supra-threshold amplitudes. These results complemented the analysis of Fig. 5A, revealing that the amount of feedforward and bidirectional information was monotonically associated with the stimulus amplitude. Overall, feedforward and bidirectional information was enhanced by the stimulus presence and they could convey information about the stimulus amplitude.

Influence of task context in thalamo-cortical directional information

We showed above that for most recorded VPL-S1 neuron pairs there was more feedforward than feedback information during the first half (250 ms) of the stimulus-present trials. This differentiated amount of *DI* was related exclusively to sensory information processing, but whether it was also influenced by the task's context, remained unknown. To investigate this question, we applied our directionality analysis to a control task in which the monkey was passively stimulated by the same set of tactile stimuli, but no perceptual report was required. Using task-balanced data sets (SI Appendix), we repeated some of the previous analyses for stimulus-present trials (neuron pairs = 36, trials = 1307 hits) and stimulus-absent trials (neuron pairs = 36, trials = 1364 control rejects) in both task conditions, exploring potential differences in the percentage of *DI* when the monkey was passively stimulated (Fig. 6). Based on the previous analysis of amplitude modulation (Fig. 5), we restricted our analysis during stimulus-present trials to near-threshold and supra-threshold

amplitudes for feedforward information (neuron pairs = 36, trials = 1105 hits) and supra-threshold amplitudes for feedback and bidirectional information (neuron pairs = 36, trials = 932 hits).

We first revisited the firing rate of single neurons in VPL and S1 (17,18) and found that the average (over neurons) firing rate of each area was not substantially altered during the time course of the passive stimulation task (Fig. 6A). Consistent with this quantification, we thereafter analyzed the percentage of *DI* during the passive condition over all neuron pairs that had been recorded in both task conditions. For these paired samples, we outlined task intervals where the difference was significant and the effect size was larger than 0.3. In general, our analysis revealed task-specific variations at the level of *DI*, which occurred around the stimulus period for stimulus-present trials (left panels of Fig. 6B-D). Compared with the vibrotactile task, the arrival of the (supra-threshold) stimulus in passive trials produced a lesser increase of bidirectional information (neuron pairs = 36; Fig. 6D left) during the second half of the stimulus window and a specific increase of feedback information during the first 250 ms of the post-stimulation window (neuron pairs = 36; Fig. 6C left). Notably, feedforward information was significantly higher in the active than the passive condition, both during the stimulus period (left panel of Fig. 6B) and PWS (right panel of Fig. 6B). Thus, our findings show that *DI* across VPL-S1 neuron pairs was sensitive to the task context. In particular, passive stimulation mitigated the amount of bidirectional information during stimulus delivery while enhancing feedback information with a certain delay.

Influence of the task on zero-lag interactions

A priori, we defined *DI* types by matching the location of driver or target neurons to either VPL, S1 or both. However, the characterization of the *DI* delays presented in Fig. S2 (SI Appendix) unraveled features that could give rise to new characterizations. More specifically, the large percentage of bidirectional information occurring at zero delay (≥33%; Fig S2B) suggested that the zero-delay case could partially explain the trends reported for the bidirectional type. To study this question in detail, we decomposed bidirectional information into two sub-types:

zero-lag, for which both statistics (one per direction) were significant at zero delay, and non-zero lag, for which both statistics were simultaneously significant at non-zero delays (SI Appendix). We repeated most of the previous analyses on these two sub-types (Fig. 7). To begin with, we represented the time-varying percentage of each *DI* subtype during the time course of the task (Fig. 7A). Crucially, Fig. 7A shows that only zero-lag bidirectional information was significantly increased during the first 250 ms of the stimulus period ($P < 0.05$, $H > 0.14$; left panel of Fig. 7A) and hence the reported overall bidirectional increase ($H = 0.1$; Fig. 7A left) was due to the zero-delay sub-type. We then related zero-lag and non-zero lag bidirectional information with the firing rate of neurons in VPL and S1 ($n = 53$ and $n = 75$, respectively; Fig. 7B and C). The results highlight that the firing rate of neurons holding zero-lag bidirectional information was frequently larger than those with non-zero lag (Wilcoxon rank-sum test, $P < 0.05$). Nonetheless, Fig S7A and B validated that this enhancement of the firing rate did not simply follow from a larger correlation between the firing rate and zero-lag bidirectional information as compared to other *DI* types (Spearman's rho<0.2). Another reported feature of bidirectional information was its monotonic association with the stimulus amplitude (Fig. 5 and SI Appendix, Fig. S7C left). Hence, in light of the new decomposition, we investigated the contribution of the zero-lag sub-type to this trend. Performing the same analysis of Fig. 5B, we found that the modulation of bidirectional information by the stimulus amplitude was mostly explained by zero-lag bidirectional information (trials = 7587, $r = 0.06$ in neuron pairs = 84, $R=0.81$, $P < 0.05$; SI Appendix, Fig. S7B). Finally, we investigated the influence of the task context into zero-lag bidirectional information (Fig. 7D). In line with our previous analysis (Fig. 6D), we considered supra-threshold amplitudes (neuron pairs = 36, trials = 932 hits) and compared the amount of zero-lag bidirectional information across the same neurons pairs in both tasks. Critically, as compared to the original task ($P < 0.05$), zero-lag bidirectional information was not altered by the stimulus presence during passive stimulation. In contrast, this context effect was not observed in non-zero-lag bidirectional information. Taken together, we concluded that the distinctive features of bidirectional information reported so far were essentially

occurring at zero delay. For the sake of interpretability, zero-lag bidirectional information will be referred to hereafter in short as zero-lag interaction.

Feedforward information correlates with the animal's task performance

An important question is whether the *DI* across VPL-S1 neuron pairs is modulated by the animal's task performance. To further examine this question, we first analyzed the differences between hit and miss trials during stimulus-present condition (left panel of Fig. 8A) and between correct rejections and false alarm trials during stimulus-absent trials (right panel of Fig. 8A) across single neuron firing rates (Fig. 8A) and *DI* types (Fig. 8B-D). In stimulus-present trials, we controlled for the effect of stimulus amplitudes by analyzing the difference between hits and misses at the near-threshold amplitude value (9 μm), where the number of samples was the most balanced between hit (trials = 443 hits in neuron pairs = 79) and miss responses (trials = 389 misses in neuron pairs = 79). In both experimental conditions, we controlled for a possible sample bias and experimental sessions effect, by using group-based permutation tests at the level of neuron pairs (SI Appendix). We then outlined task intervals where the difference was significant and the effect size was larger than 0.2. Our analysis primarily revealed that the amount of feedforward information during the first half of the stimulus period in stimulus-present trials was significantly larger ($P < 0.05$, $H > 0.2$) in hit trials (left panel of Fig. 8A). In contrast, our data did not unravel strong significant differences between correct rejections and false alarms during stimulus-absent trials (trials = 4188 correct rejections and false alarm trials = 933 in neuron pairs = 82; right panel of Fig. 8A). Overall, our results indicate that the amount of feedforward information during the first half of the stimulus window was correlated with the monkey's behavior and could potentially predict the monkey's performance in stimulus-present trials (left panel of Fig. 8B).

DISCUSSION

Here, we sought to determine the functional roles of thalamo-cortical information flows in perception at a fine temporal scale. This was done by estimating a directional information measure (referred to as *DI*) between simultaneously recorded VPL-S1 neuron pairs sharing the same cutaneous receptive field, while monkeys

performed a vibrotactile detection task. Notably, the estimated *DI* could not be merely explained by increases in the firing rates of neurons within VPL or S1 during the stimulus period. We found that the stimulus presence elicited a significant increment on the amount of feedforward information (VPL→S1) and zero-lag interaction. In contrast, pure feedback (S1→VPL) information remained practically unaltered during the stimulus presence. Remarkably, increments in feedforward and zero-lag interaction were differently modulated as a function of the stimulus amplitude. Although we found a monotonic relationship between both feedforward and zero-lag interaction and the stimulus amplitude, zero-lag interaction only emerged significantly with supra-threshold sensory inputs during task performance. Additionally, we identified that thalamic and cortical neurons involved in bidirectional information exhibited higher firing rates during stimulus presence. Interestingly, the amount of feedforward information was correlated with the monkeys' performance when they judged the presence at near-threshold stimuli. Also, during a passive stimulation task, when the monkeys were not required to report their percepts, both feedforward information and, more prominently, zero-lag interaction were reduced during the stimulus presence. This suggests that feedforward information and zero-lag interaction are modulated by the task-context. We discuss these findings below.

In the current study, we extended previous spectral and neural population studies on thalamo-cortical directionality (10, 27-29) to the temporal domain, at the level of single-neuron activity. To achieve this, we analyzed the *DI* between VPL and S1 neuronal spike trains with a nonlinear measure (5,19,20). Indeed, we decomposed single-neuron *DI* into three types: feedforward, feedback and bidirectional, and explored their temporal evolution from the pre-stimulus up to the post-stimulus intervals of the detection task. In particular, the lack of pure feedback modulation (i.e. not concurrent to feedforward information) during the stimulus period, suggests that the spike-field coherence (SFC) increment in the S1→VPL direction shown in (29) could be associated with increments in zero-lag interaction. Our data analysis approach involved the use of nonparametric significance tests (30) and the choice of the percentage of significant *DI* estimates as a relevant connectivity metric (5). Both

choices were critical to detect nonlinear spike-train temporal correlations in a way that was shown to be weakly dependent on the firing rate in real and simulated data. As a result, we were able to analyze neuronal data in a dimension that was quasi-orthogonal to the firing rates (17,18), while still showing rich stimulus modulations. Besides, it is important to mention the differences between the *DI* measure used here with the widespread measure of noise correlation (31,32). Noise correlation averages across trials under the same stimulus condition, correlating fluctuations in firing rate of two neurons. In contrast, *DI* quantifies, in a single trial and for any given time, the information that the recent past and present spike train of a given neuron has about the present spike train of the other, simultaneously recorded, neuron.

Notably, feedforward VPL-S1 information was modulated during the stimulus period. Further, the modulation was stronger during the first half of the stimulus period (250ms). These findings are congruent with the adaptation of feedforward information over the stimulus period. Indeed, previous studies have shown that thalamic and cortical neurons become adapted to tactile stimuli after several pulses (17,18,33). Moreover, it has been reported that this adaptation changes the neural code of cortical neurons and thalamic synchrony from a detection to a discrimination modality (34). As stated above, our directionality measure is poorly correlated with differences in firing rate of VPL and S1 neurons. Therefore, our results are congruent with the adaptive coding paradigm (34), by showing that feedforward and zero-lag interactions exhibit the strongest modulation during the first part of the stimulus presence. In sum, we hypothesize that feedforward adaptation reflects an internal mechanism that prioritizes the information contained within the first pulses of the sinusoidal stimulus to further transmit this information to the cortex and therefore, for stimulus detection during this task.

According to the standard classification of thalamic sensory nuclei (6), VPL is considered a first-order relay nucleus that mainly transmits afferent information to S1 in the presence of cortical feedback (9,35,36). Our results support this view by showing that feedforward information alone was primarily boosted during the first 250 ms immediately after the stimulus onset. The increment in feedforward information was concentrated at a delay of 8 ms, which is consistent with previous

literature (37). Moreover, these increments were reduced during incorrect trials and, to a lesser extent, during the passive control condition. In particular, the relationship between feedforward information and the monkey's performance during stimulus-present trials is of special novelty. In previous related studies, this correlation did not arise neither in spiking activity (18) nor in the oscillatory activity (29). This result suggests that perceptual detection might be related to the amount of stimulus information flowing from VPL to S1. In contrast, pure feedback information did not display substantial task modulations. We hypothesize that pure feedback information might be relevant for perceptual detection but is generally less frequent than feedforward information. On the other hand, cortical areas and higher order thalamic nuclei (reviewed by (38)) might show more prominent feedback cortico-thalamic information, perhaps related to not only facilitating the gating of the stimulus, but also to some other cognitive aspects not detected in this task.

Our study revealed that feedback information could take place concurrently with feedforward information, suggesting the emergence of a thalamo-cortical loop, denominated here in sum as bidirectional information. In particular, our analysis identified that bidirectional information showed bimodality between those cases where *DI* simultaneously occurred at zero-delay (zero-lag interaction) and those cases at non-zero delay. Crucially, only zero-lag interaction was modulated by the stimulus presence, involved neurons exhibiting higher firing rates than in the unidirectional case and was significantly diminished in the passive stimulation task. Hence, zero-lag interaction conveyed both stimulus and contextual information, thus indicating that its mechanism might be different from the non-zero subtype. Unlike the feedforward type, we suggest that zero-lag interaction may not reflect direct routing of information (39). Instead, it could be established by common inputs from mediating cortical neurons. In particular, it will be interesting in future studies to simultaneously record the activity of higher–order areas like prefrontal cortex to examine how common cortical inputs driving zero-lag interactions (40) are associated with the expectancy caused by different pre-stimulus period times, a variable that was led out of the scope here. Here, we consider that the task-context modulation of zero-lag interaction requires the engagement of downstream cortical areas in this loop. Specifically, in

concordance with computational models supporting zero-lag brain inter-area synchronization (42-44), we propose that zero-lag interaction could be originated by a top-down modulation of cortical areas establishing a similarly delayed reciprocal loop with both S1 and the thalamus (9, 45).

Recently, a study in monkeys performing a visual detection task was also able to relate the propagation of neural activity along the visual pathway with the monkey's detection accuracy (46). The authors showed that information about unreported stimuli may be lost at any stage of the pathway (V1-V4-PFC) with an overall excursion that depended on the stimulus strength. Despite the methodological differences with the study presented here (the authors recorded cortical areas along the visual pathway, analyzed multi-unit activity (MUA) instead of single-unit activity, indirectly measured activity propagation via local MUA, and used microstimulation, among others), their results suggest that stimulus perception of near-threshold stimuli may depend on the feedforward information flow across the early stages of the sensory pathway. More specifically, they explain their results with a model involving thalamo-cortical and cortico-cortical propagation, but no cortico-thalamic projections. While our main findings may fit in this model (see also (3)), the task modulation of zero-lag interaction between VPL and S1 suggests the additional existence of indirect cortico-thalamic pathways towards VPL in the somatosensory model.

In brief, the present study employed a fine-temporal methodology supporting that the increment of VPL→S1 neuronal *DI* (as opposed to S1→VPL) at around 8ms during the stimulus period, may reflect the effective transmission of tactile information from thalamus to cortex. Indeed, it suggests that the amount of feedforward information occurring during the first 250 ms of stimulation correlates with the monkey's stimulus perception and with the behavioral task performance. Meanwhile, zero-lag interaction, which was reduced when monkeys did not require to report stimulus presence, may reflect the top-down modulation of the cortico-thalamic circuitry needed for stimulus perception. Our results, therefore, contribute to understanding the *DI* flow between the VPL and S1 during the detection of a tactile stimulus. Finally, the minimalistic approach used here; that is, the

simultaneous recording of VPL-S1 neuron pairs sharing the same receptive field, together with the estimation of *DI* flow, could be used to not only investigate the functional role of the thalamo-cortical *DI* during perception, but also across other brain areas in this and in other behavioral tasks.

MATERIALS AND METHODS

Monkeys were trained to report whether or not they felt the stimulus (SI Appendix). Neuronal recordings were obtained in VPL and S1 while the monkeys performed the detection task. Directional information was calculated between neuron pairs simultaneously recorded in VPL and S1 (SI Appendix). Animals were handled in accordance with standards of the National Institutes of Health and Society for Neuroscience. All protocols were approved by the Institutional Animal Care and Use Committee of the Instituto de Fisiología Celular, Universidad Nacional Autónoma de México.

ACKNOWLEDGMENTS

This work was supported in part by the Dirección General de Asuntos del Personal Académico de la Universidad Nacional Autónoma de México (PAPIIT-IN210819) and Consejo Nacional de Ciencia y Tecnología (CONACYT-240892) (R.R.). Support for this work was provided by European project FP7-ICT BrainScales (G.D.). In addition, G.D. was supported by the European Research Council Advanced Grant: DYSTRUCTURE (n. 295129), by the Spanish Research Project SAF2010-16085. Y.V. was supported by a Pew Latin American Fellowship and a Charles H. Revson Biomedical Science Fellowship.

REFERENCES

1. Salinas, E., Hernández, A., Zainos, A., and Romo, R. (2000). Periodicity and firing rate as candidate neural codes for the frequency of vibrotactile stimuli. J. Neurosci. *20*, 5503–5515.
2. de Lafuente, V., and Romo, R. (2005). Neuronal correlates of subjective sensory experience. Nat. Neurosci. *8*, 1698–1703.
3. de Lafuente, V., and Romo, R. (2006). Neural correlate of subjective sensory experience gradually builds up across cortical areas. Proc. Natl. Acad. Sci. USA *103*, 14266–14271.

4. Hernández, A., Nácher, V., Luna, R., Zainos, A., Lemus, L., Alvarez, M., Vázquez, Y., Camarillo, L., and Romo, R. (2010). Decoding a perceptual decision process across cortex. Neuron *66*, 300-314.
5. Tauste Campo, A., Martinez-Garcia, M., Nácher, V., Luna, R., Romo, R., and Deco, G. (2015). Task-driven intra- and interarea communications in primate cerebral cortex. Proc. Natl. Acad. Sci. USA *112*, 4761–4766.
6. Sherman, S.M. (2016). Thalamus plays a central role in ongoing cortical functioning. Nat. Neurosci. *19*, 533–541.
7. Alitto, H.J., and Usrey, W.M. (2003). Corticothalamic feedback and sensory processing. Curr. Opin. Neurobiol. *13*, 440–445.
8. Briggs, F., and Usrey, W.M. (2007). A fast, reciprocal pathway between the lateral geniculate nucleus and visual cortex in the macaque monkey. J. Neurosci. *27*, 5431–5436.
9. Crandall, S.R., Cruikshank, S.J., and Connors, B.W. (2015). A Corticothalamic Switch: Controlling the Thalamus with Dynamic Synapses. Neuron *86*, 768–782.
10. Wang, J.Y., Chang, J.Y., Woodward, D.J., Baccalá, L.A., Han, J.S., and Luo, F. (2007). Corticofugal influences on thalamic neurons during nociceptive transmission in awake rats. Synapse *61*, 335–342.
11. Jones, E.G. (2002). Thalamic circuitry and thalamocortical synchrony. Philos. Trans. R. Soc. B Biol. Sci. *357*, 1659–1673.
12. Sherman, S.M., and Guillery, R.W. (2006). Exploring the Thalamus and Its Role in Cortical Function (Cambridge, MA: The MIT Press).
13. Alonso, J.M., Usrey, W.M., and Reid, R.C. (1996). Precisely correlated firing in cells of the lateral geniculate nucleus. Nature *383*, 815–819.
14. Ahissar, E., Sosnik, R., and Haidarliu, S. (2000). Transformation from temporal to rate coding in a somatosensory thalamocortical pathway. Nature *20*, 302-306.
15. Bruno, R.M., and Sakmann, B. (2006). Cortex Is Driven by Weak but Synchronously Active Thalamocortical Synapses. Science *312*, 1622–1627.

16. Bruno, R.M. (2011). Synchrony in sensation. Curr. Opin. Neurobiol. *21*, 701–708.
17. Vázquez, Y., Zainos, A., Alvarez, M., Salinas, E., and Romo, R. (2012). Neural coding and perceptual detection in the primate somatosensory thalamus. Proc. Natl. Acad. Sci. USA *109*, 15006–15011.
18. Vázquez, Y., Salinas, E., and Romo, R. (2013). Transformation of the neural code for tactile detection from thalamus to cortex. Proc. Natl. Acad. Sci. USA *110*, E2635-E2644.
19. Massey, J. (1990). Causality, feedback and directed information. In Proc. Int. Symp. Inf. Theory Applic. 27–30.
20. Jiao, J., Permuter, H.H., Zhao, L., Kim, Y.H., and Weissman, T. (2013). Universal estimation of directed information. In IEEE Trans. on Inform. Theory *59*, 6220–6242.
21. Winkler, A.M., Ridgway, G.R., Webster, M.A., Smith, S.M., Nichols, T.E. (2014). Permutation inference for the general linear model. Neuroimage *92*, 381-397.
22. Cohen, J. (1988). Statistical power analysis for the behavioral sciences. Stat. Power Anal. Behav. Sci. *2*, 567.
23. Carnevale, F., deLafuente, V., Romo, R., Barak, O., and Parga, N. (2015). Dynamic Control of Response Criterion in Premotor Cortex during Perceptual Detection under Temporal Uncertainty. Neuron *86*, 1067–1077.
24. Deschênes, M., Veinante, P., and Zhang, Z.W. (1998). The organization of corticothalamic projections: Reciprocity versus parity. Brain Res. Rev. *28*, 286–308.
25. Pipa, G., Wheeler, D. W., Singer, W., and Nikolic, D. (2008). Neuroxidence: reliable and efficient analysis of an excess or deficiency of joint-spike events. J. Neurosci. Methods 25, 64–88.
26. Louis, S., Gerstein, G. L., Grün, S., and Diesmann, M. (2010). Surrogate spike train generation through dithering in operational time. Front. Comput. Neurosci. 4:127.

27. FitzGerald, T., Valentin, A., Selway, R., and Richardson, M.P. (2013). Cross-frequency coupling within and between the human thalamus and neocortex. Front. Hum. Neurosci. *7*, 7-84.
28. Bastos, A. M., Briggs, F., Alitto, H. J., Mangun, G. R., and Usrey, W. M. (2014). Simultaneous recordings from the primary visual cortex and lateral geniculate nucleus reveal rhythmic interactions and a cortical source for gamma-band oscillations. J. Neurosci. *34*, 7639-7644.
29. Haegens, S., Vázquez, Y., Zainos, A., Alvarez, M., Jensen, O., and Romo, R. (2014) Thalamocortical rhythms during a vibrotactile detection task. Proc. Natl. Acad. Sci. USA *111*, E1797-1805.
30. Gilson, M., Tauste Campo, A., Thiele, A., and Deco, G. (2017). Non-parametric test for connectivity detection in multivariate autoregressive networks and application to multiunit activity data. Net. Neurosci. *1*, 357-380.
31. Ecker, A.S., Berens, P., Cotton, R.J., Subramaniyan, M., Denfield, G.H., Cadwell, C.R., Smirnakis, S.M., Bethge, M., and Tolias, A.S. (2014). State dependence of noise correlations in macaque primary visual cortex. Neuron *82*, 235-248.
32. Kohn, A., Coen-Cagli, R., Kanistscheider, I., and Pouget, A. (2016). Correlations and neuronal population information. Ann. Rev. Neurosci. *39*, 237-256.
33. Khatri, V., Hartings, J.A., and Simons, D.J. (2004). Adaptation in Thalamic Barreloid and Cortical Barrel Neurons to Periodic Whisker Deflections Varying in Frequency and Velocity. J. Neurophysiol. *92*, 3244–3254.
34. Wang, Q., Webber, R.M., and Stanley, G.B. (2010). Thalamic synchrony and the adaptive gating of information flow to cortex. Nat. Neurosci. *13*, 1534–1541.
35. Blomquist, P., Devor, A., Indahl, U.G., Ulbert, I., Einevoll, G.T., and Dale, A.M. (2009). Estimation of thalamocortical and intracortical network models from joint thalamic single-electrode and cortical laminar-electrode recordings in the rat barrel system. PLoS Comput. Biol. *5*, E10003285.

36. Ahissar, E., and Oram, T. (2015). Thalamic relay or cortico-thalamic processing? Old question, new answers. Cereb. Cortex *25*, 845-848.
37. Briggs, F., and Usrey, W.M. (2008). Emerging views of corticothalamic function. Curr. Opin. Neurobiol. *18*, 403–407.
38. Halassa, M.M. and Kastner, S. (2017) Thalamic functions in distributed cognitive control. Nat. Neurosci. *20*, 1669-1679.
39. Besserve, M., Lowe, S. C., Logothetis, N. K., Schölkopf, B., & Panzeri, S. (2015). Shifts of gamma phase across primary visual cortical sites reflect dynamic stimulus-modulated information transfer. *PLoS Biol.*, *13*, e1002257.
40. Riehle, A., Grün, S., Diesmann, M., Aertsen, A. (1997). Spike synchronization and rate modulation differentially involved in motor cortical function. Science, 278(5345), 1950-1953.
41. Constantinople CM & Bruno RM. (2013) Deep cortical layers are activated directly by thalamus. Science. *340*, 1591-1594.
42. Fischer, I., Vicente, R., Buldú, J.M., Peil, M., Mirasso, C.R., Torrent, M.C., García-Ojalvo, J. (2006) Zero-lag long-range synchronization via dynamical relaying. Phys. Rev. Lett. *97*, 123902.
43. Vicente, R., Gollo, L.L., Mirasso, C.R., Fischer, I., and Pipa G. (2008). Dynamical relaying can yield zero time lag neuronal synchrony despite long conduction delays. Proc. Natl. Acad. Sci. USA *105*, 17157-17162.
44. Gollo L.L., Mirasso C., Sporns O., and Breakspear M. (2014) Mechanisms of zero-lag synchronization in cortical motifs. Plos Comput. Biol. *10*, e1003548.
45. Collins, D.P., Anastasiades, D.J., Marlin, J.J., and Carter, A.G. (2018) Reciprocal circtuits linking prefrontal cortex with ventral and dorsal thalamic nuclei. Neuron *98*, 366-379.
46. van Vugt, B., Dagnino, B., Vartak, D., Safaai, H., Panzeri, S., Dehaene, S., and Roelfsema, P.R. (2018). The threshold for conscious report: Signal loss and response bias in visual and frontal cortex. Science *360*, 537-542.

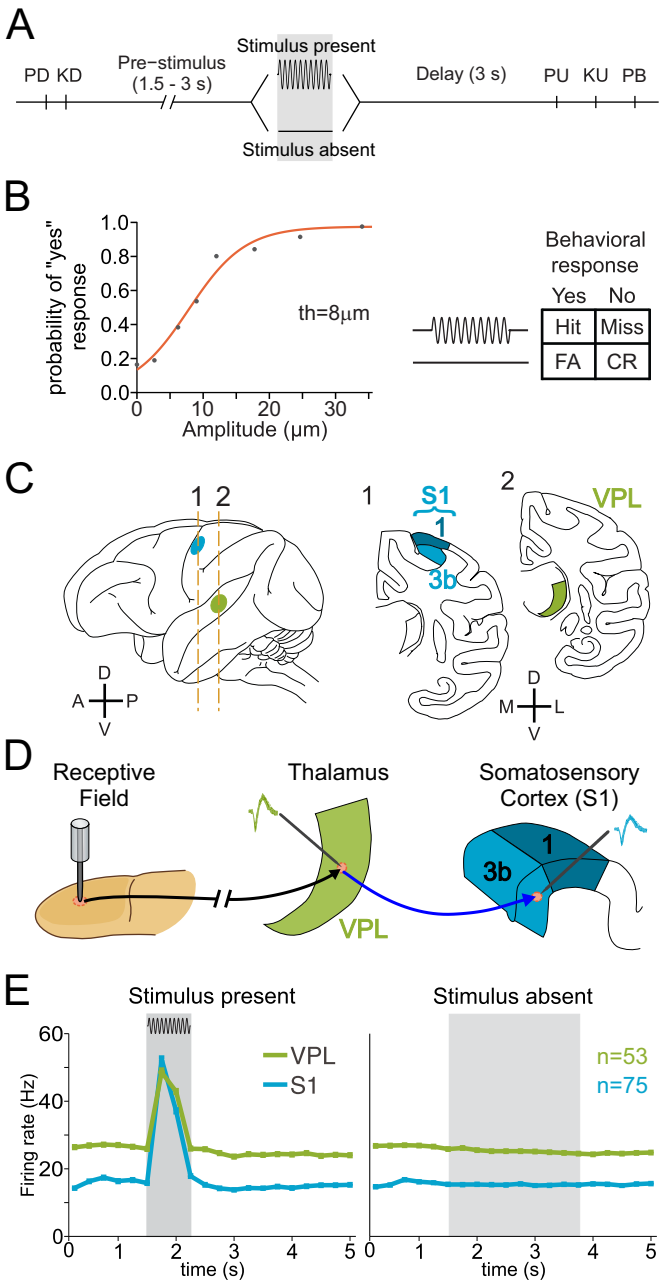

Figure 1. Detection task, psychophysical performance, recording sites and neuronal responses during the task. (A) Vibrotactile detection task. Trials began when the stimulator probe indented the skin of one fingertip of the monkey's restrained right hand (probe down, PD); the monkey reacted by placing its left, free hand on an immovable key (key down, KD). After a variable pre-stimulus period (1.5 – 3 s), a vibratory stimulus of variable amplitude (1−34 µm, 20 Hz, 0.5 s duration) was presented on one half of the trials; no stimulus was presented on the other half of the trials. Following the stimulus presentation period or a period where no stimulus was delivered, the monkey waited for 3 s until the probe was lifted off from the skin (PU, probe up); then the animal removed its free hand from the key (KU, key up) and pressed one of two push buttons (PBs) to report whether the stimulus was present or absent. Lateral and medial buttons were used for reporting stimulus-presence and stimulus-absence, respectively. Stimulus-present and stimulus-absent trials were randomly interleaved within a run. (B) The button pressed indicated whether the monkey felt the stimulus (henceforth referred as 'yes' and 'no' responses, respectively). Left panel in B: mean psychometric function depicting the probability of the monkey reporting 'yes' as a function of the stimulus amplitude (th = 8 µm, detection threshold). Right panel in B: behavioral responses depending on the stimulus-presence (Hit or Miss) or stimulus-absence (CR, correct rejection; FA, false alarm). (C) Recording sites in the ventral posterior lateral (VPL) nucleus (green) of the thalamus and in areas 1 and 3b of the primary somatosensory cortex (S1, cyan). (D) Scheme depicting how the neural activity from single neurons in the VPL and S1 (3b or area 1) sharing the same cutaneous receptive field was simultaneously recorded during the detection task. (E) Mean firing rate for the simultaneously recorded VPL (n = 53) and S1 (n = 75) neurons during the stimulus-present and stimulus- absent trials.

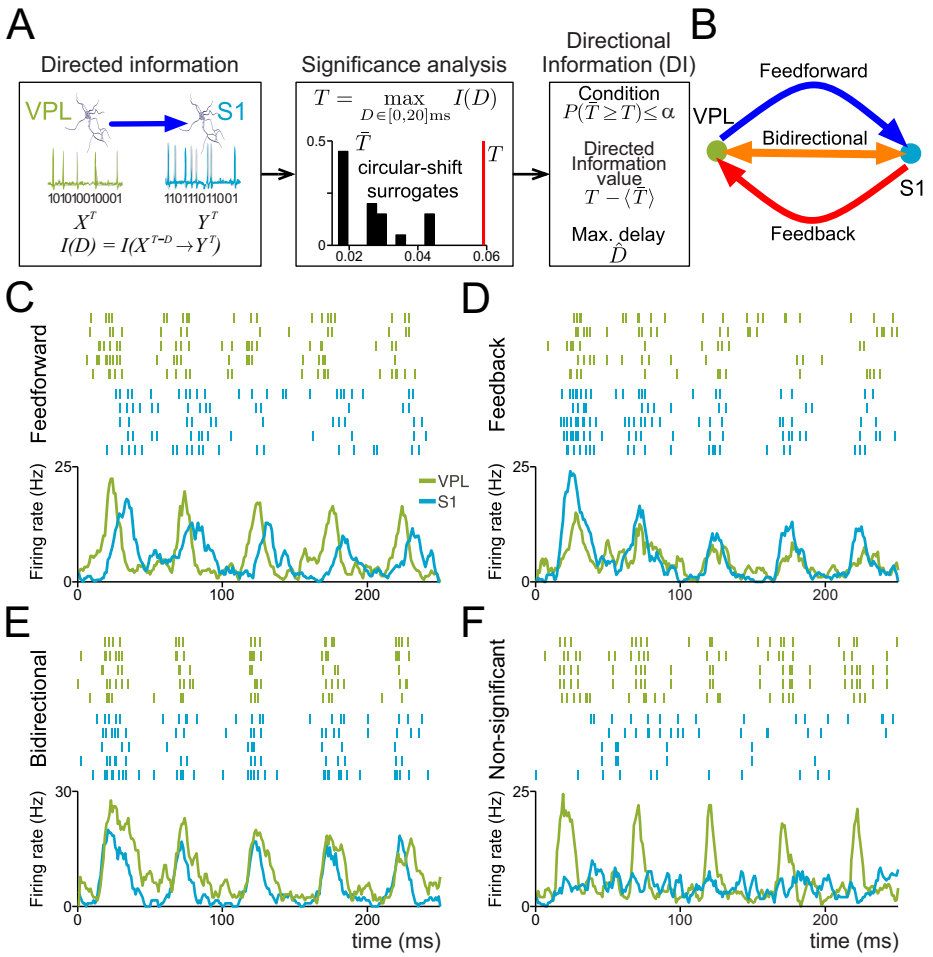

Figure 2. Assessing directional information (DI) between pairs of VPL and S1 neurons during the detection task. (A) Sequential scheme representing the method to infer single-trial DI. Left panel: directed information is estimated between single-trial spike trains of the simultaneously recorded neurons in VPL and S1 for delays (0, 2,…, 20) ms. Middle panel: significance is locally determined via non-parametric testing ($\alpha = 0.05$) of a maximizing-delay statistic. Right panel: every significant statistic is associated with an unbiased directed information value (T-‹T›) and a maximizing delay ($\hat{D}$). (B) Graphical representation for feedforward (VPL→S1, in blue), feedback (S1→VPL, in red) and bidirectional (S1↔VPL, in orange) information between VPL and S1 neurons. (C-F) Raster plots and spike density functions depicting the neural activity occurring during the first 250 ms of stimulation (34 µm) for examples of VPL (green) and S1 (cyan) neuron pairs involved in feedforward (C), feedback (D), bidirectional (E) information, and non-significant (F) statistic values.

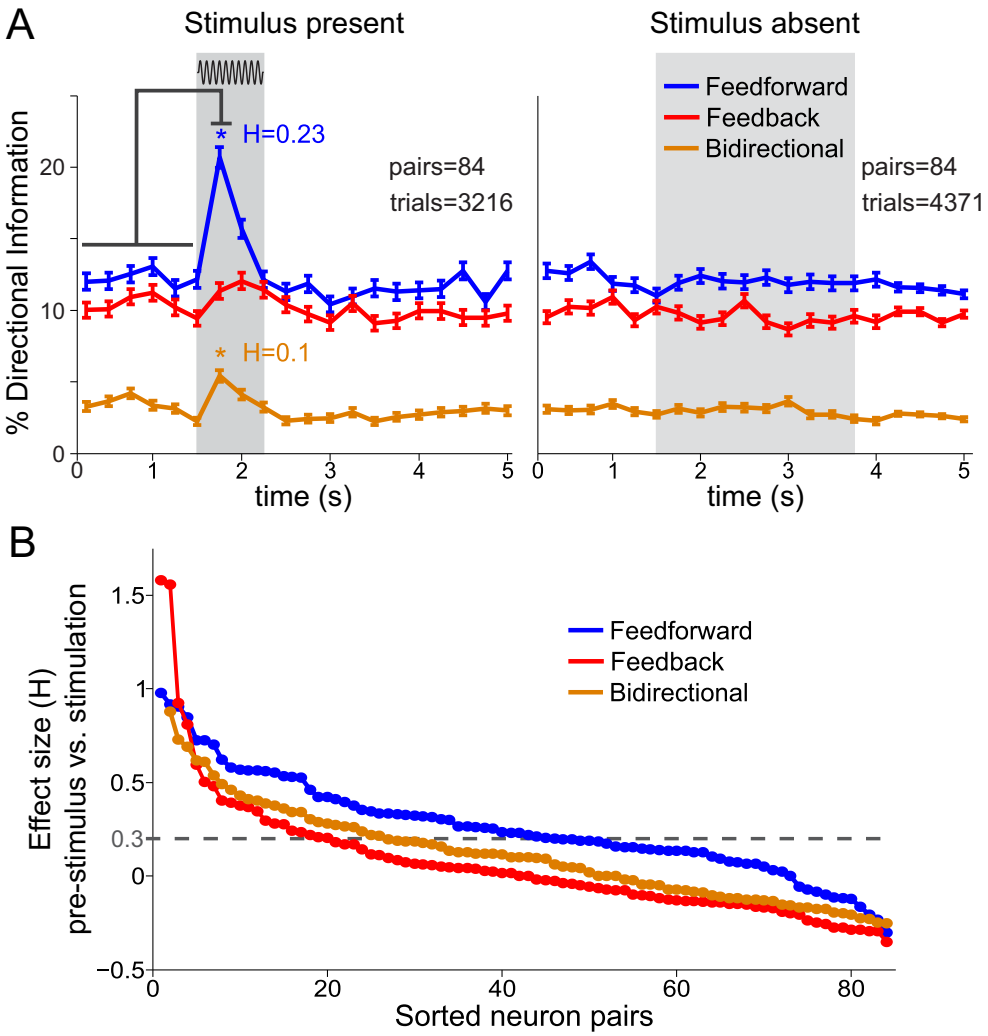

Figure 3. VPL-S1 feedforward, feedback and bidirectional information during the detection task. We analyzed hit and correct rejection trials across all recorded VPL-S1 neuron pairs. (A) Percentage of feedforward, feedback and bidirectional information during the time course of the task during the stimulus-present (left panel, trials = 3216 hits; neuron pairs = 84) and stimulus-absent trials (right panel, trials = 4371 correct rejections; neuron pairs = 84). Error bars denote the SEM (standard error of the mean). In all figures, gray boxes depict the stimulation period for the stimulus-present trials, and the possible window of stimulation (PWS) for the stimulus-absent trials. Asterisks denote significant differences ($P < 0.05$) between the pre-stimulus (first 6 task intervals, 1.5 s) and the first half (0-0.25 s) of the stimulus period (non-parametric test, $\alpha = 0.05$). H denotes the effect size and average effect size (Cohen's H) of significant differences. (B) Effect size of the difference between the percentage of each DI type during the pre-stimulus period and during the first stimulation interval as a function of all neuron pairs for distinct DI. Each plot is represented by ordering the neuron pairs in descending order according to the magnitude of the effect size for each particular DI type. The black horizontal dashed line represents the effect size threshold ($H \geq 0.3$).

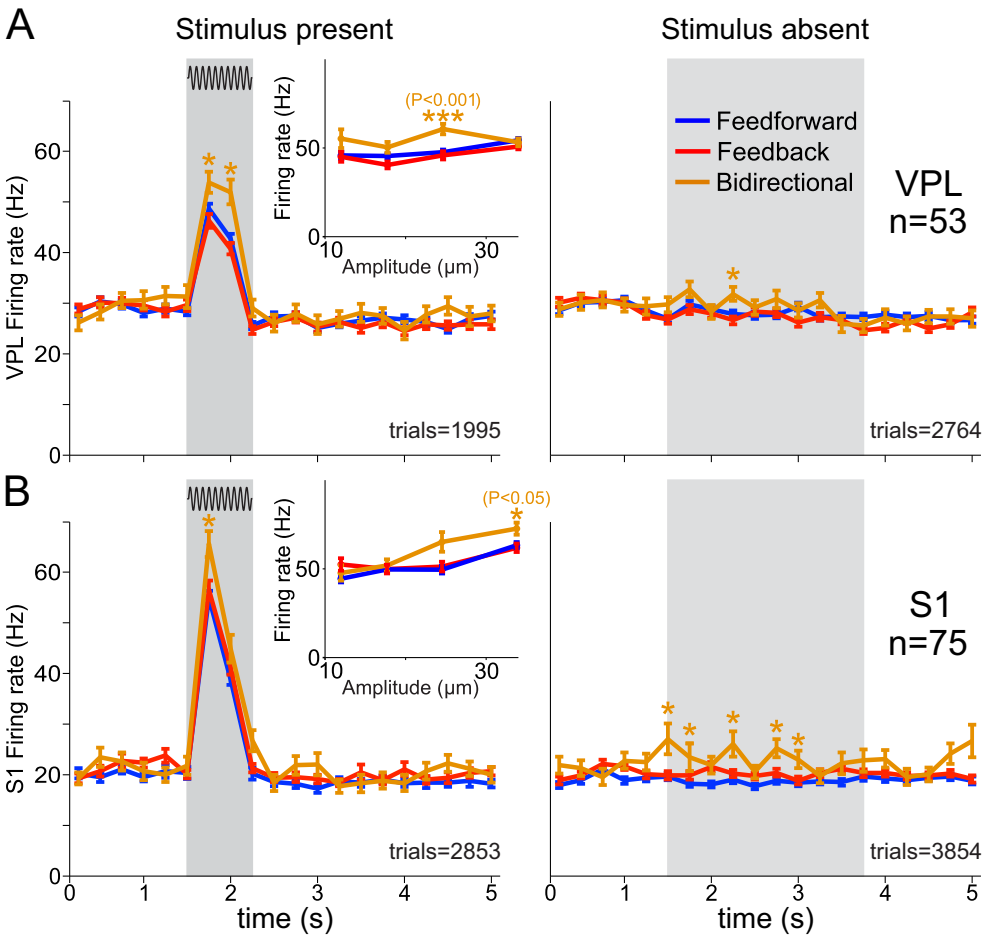

Figure 4: Mean firing rate of VPL and S1 neurons during detection task for feedforward, feedback and bidirectional information. We analyzed hit and correct rejection trials across all recorded neurons in VPL and S1. For all panels, gray boxes depict the stimulation period for the stimulus-present trials (left panels), and the possible window of stimulation (PWS) for the stimulus-absent trials (right panels). Blue, red and orange traces depict the mean firing rate for neurons holding feedforward, feedback and bidirectional information, respectively, during the time course of the detection task (neuron pairs = 84). Error bars denote the SEM (standard error of the mean). (A) Mean firing rate for VPL neurons (n = 53; left panel, trials = 1995 hits; right panel, trials = 2764 correct rejections). Insets depict the mean firing rate as a function of the stimulus amplitude. Asterisks denote significant differences (*, P<0.05, Wilcoxon rank-sum test) among the firing rate of neurons holding distinct DI. (B) Similar as panel A, but for S1 neurons (n = 75; left panel, trials = 2853 hits; right panel, trials = 3854 correct rejections).

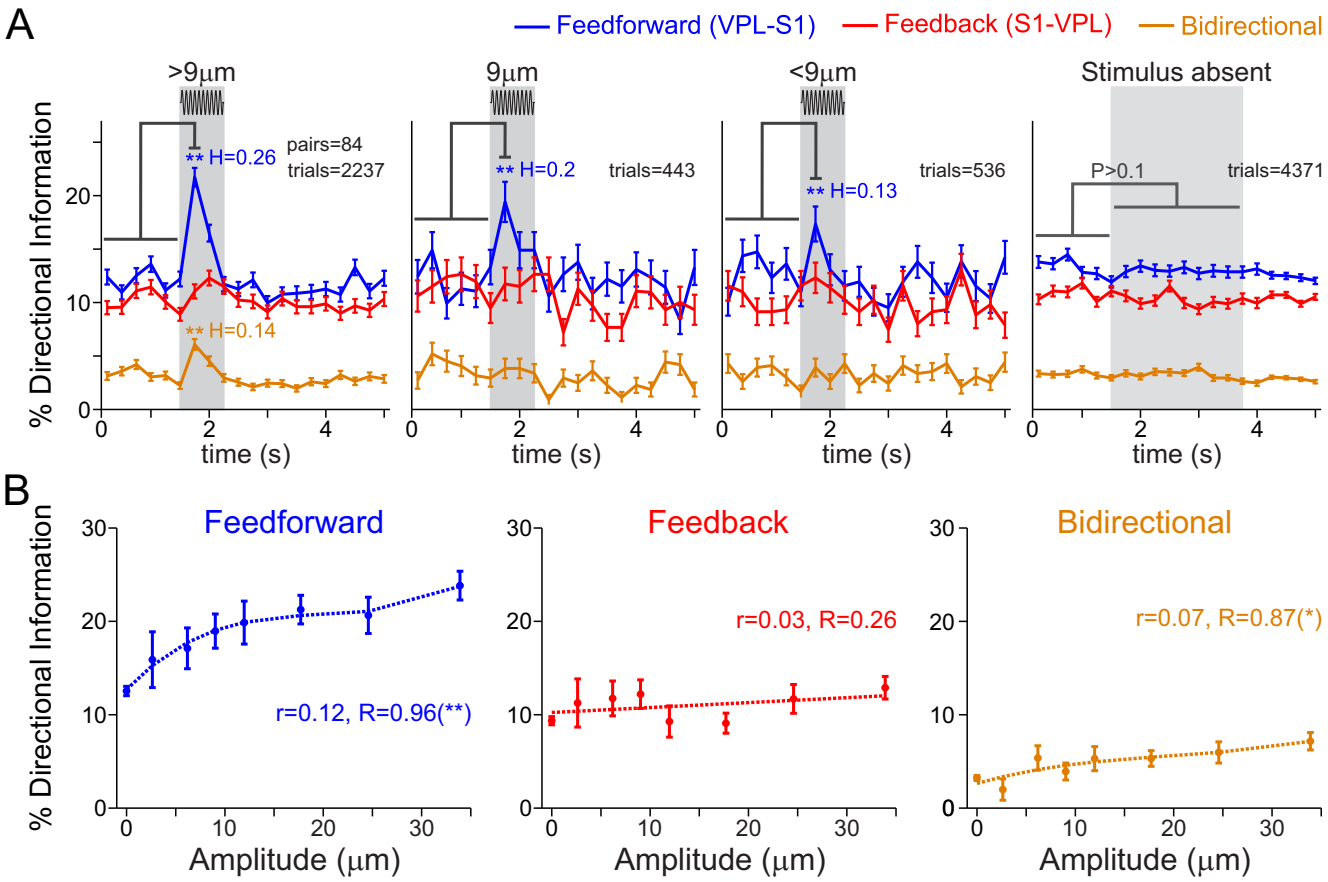

Figure 5. VPL-S1 feedforward and bidirectional information are modulated by the stimulus amplitude. We analyzed hit and correct rejection trials across all VPL-S1 neuron pairs. Hit trials were subdivided into three categories (supra-threshold, threshold and sub-threshold). (A) Time course of the percentage of feedforward (VPL→S1, blue), feedback (S1→VPL, red) and bidirectional (S1↔VPL, orange) information between VPL and S1 neurons during stimulus-present and stimulus-absent trials. From left to right: percentage of DI for supra-threshold (> 9 µm, neuron pairs = 84; trials = 2237 hits), threshold (9 µm, neuron pairs = 84; trials = 443 hits), sub-threshold (< 9 µm, neuron pairs = 84; trials = 536 hits) stimulus amplitudes and stimulus-absent trials (neuron pairs = 84; trials=4371 correct rejections). Asterisks denote significance levels (*, $P < 0.05$, **, $P < 0.01$). H denotes the effect size (Cohen's h) of significant percentage differences. Error bars denote the SEM (standard error of the mean). (B) Mean percentage of feedforward, feedback and bidirectional information as a function of the stimulus amplitude during the first half of the stimulation period (left, 0 − 0.25 s). The value of r is the correlation between the stimulus amplitude and the existence of DI in each type across all trials (no amplitude-averages) with Spearman correlation (trials = 7587). The value R is the analogous correlation considering amplitude-average values (amplitudes = 8). Asterisks depict significance (*, $P < 0.05$, **, $P < 0.01$). Error bars denote the SEM.

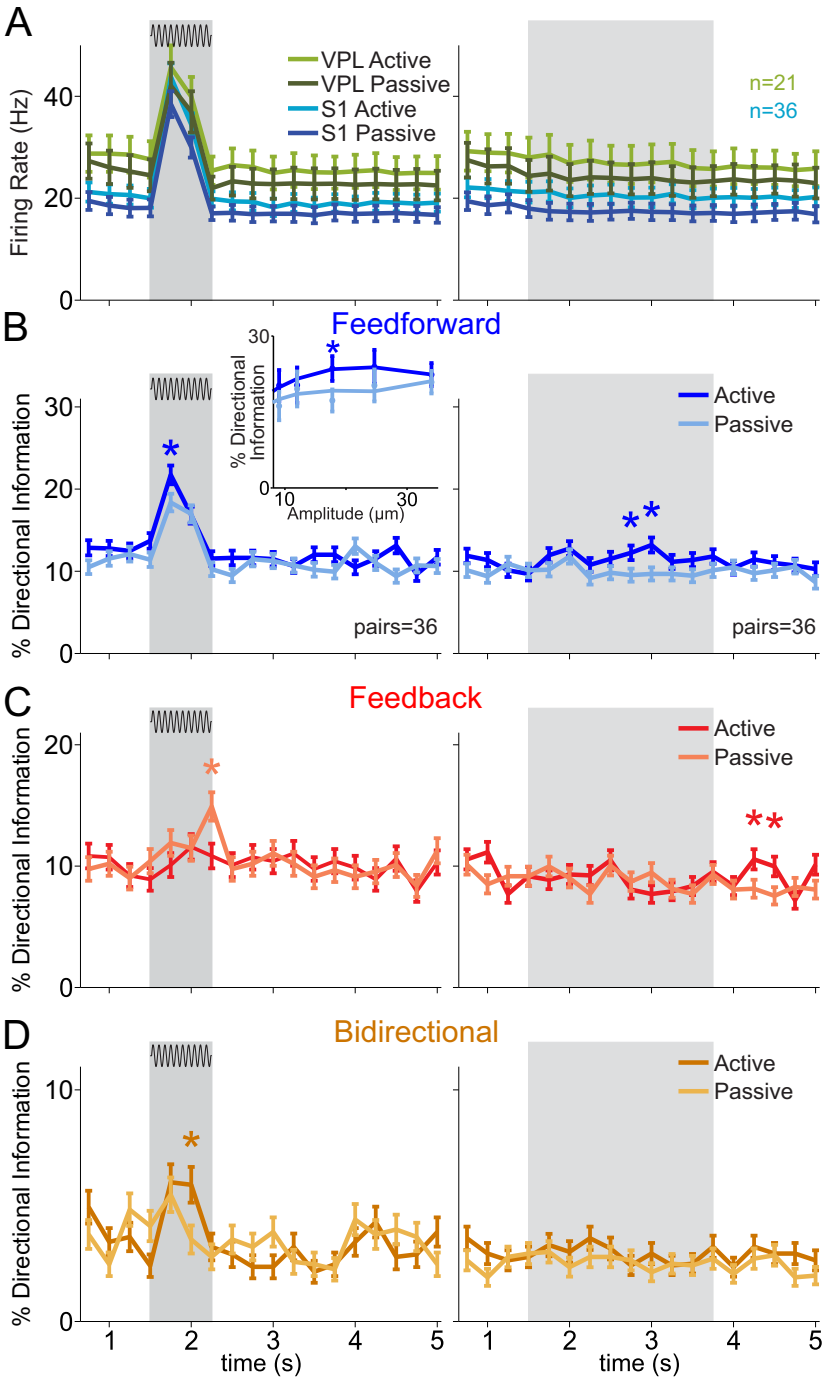

Figure 6. VPL-S1 directional information (DI) during passive stimulation. We analyzed hit and correct rejection trials across all VPL-S1 neuron pairs for feedforward information. In addition to correct rejection trials, we only analyzed supra-threshold hit trials for feedback and bidirectional information during passive stimulation, a task which did not require the animal's reports. (A) Time course of the mean firing rates for VPL (n=21) and S1 (n=36) neurons. Neuron pairs (neuron pairs=36) were simultaneously recorded during the detection task (active) and passive stimulation. For all panels, the left side depicts supra-threshold stimulus-present trials, whereas the right side depicts stimulus-absent trials. Dark and light colors depict data belonging to the active and passive conditions, respectively. (B) Time course of the percentage of feedforward information (neuron pairs=36; trials=1105 hits; trials=1364 correct rejections). (C) Time course of the percentage of feedback information for the active and passive conditions (neuron pairs=36; trials=932 hits; trials=1364 correct rejections). (D) Time course of the percentage of bidirectional information (neuron pairs=36; trials=932 hits; trials=1364 correct rejections). Inset depicts the percentage of feedforward information as a function of the stimulus amplitude. Asterisks denote significance levels (*, $P<0.05$) associated with effect sizes (Cohen's H) larger than 0.3.

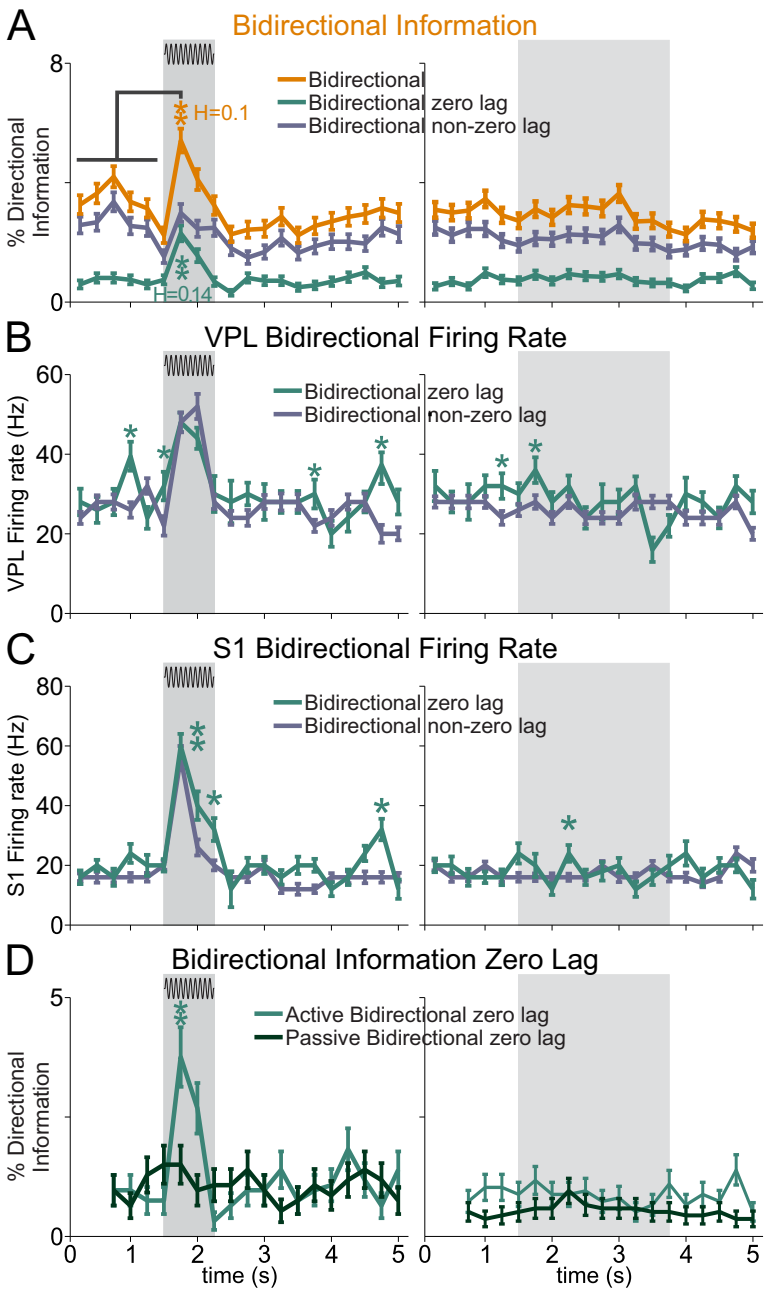

Figure 7. Distribution of bidirectional information across zero-lag and nonzero lag trials. We analyzed supra-threshold hit trials and correct rejection trials across all VPL-S1 neuron pairs. (A) Percentage of overall bidirectional information, zero-lag bidirectional information and nonzero lag bidirectional information during the time course of the task during the stimulus-present (left panel, trials = 3216 hits; neuron pairs = 84) and stimulus-absent trials (right panel, trials = 4371 correct rejections; neuron pairs = 84). Error bars denote the SEM (standard error of the mean). Asterisks denote significant differences ($P < 0.05$) between the pre-stimulus and the first stimulation interval (non-parametric test, $\alpha = 0.05$). H denotes the effect size and average effect size (Cohen's H) of significant differences. (B) Mean firing rate for VPL neurons (n = 53; left panel, trials = 1995 hits; right panel, trials = 2764 correct rejections). Asterisks denote significant differences (*, $P<0.05$, Wilcoxon rank-sum test) among the firing rate of neurons holding zero-lag and nonzero lag bidirectional information. Error bars denote the standard error of the median. (C) Similar as panel B, but for S1 neurons (n = 75; left panel, trials = 2853 hits; right panel, trials = 3854 correct rejections). (D) Time course of the percentage of zero-lag and nonzero lag bidirectional information during supra-threshold and stimulus-absent trials (neuron pairs = 36; trials = 932 hits; trials = 1364 correct rejections) during the detection task (active) and passive stimulation. Asterisks denote significance levels (*, $P<0.05$) associated with effect sizes (Cohen's H) larger than 0.3.

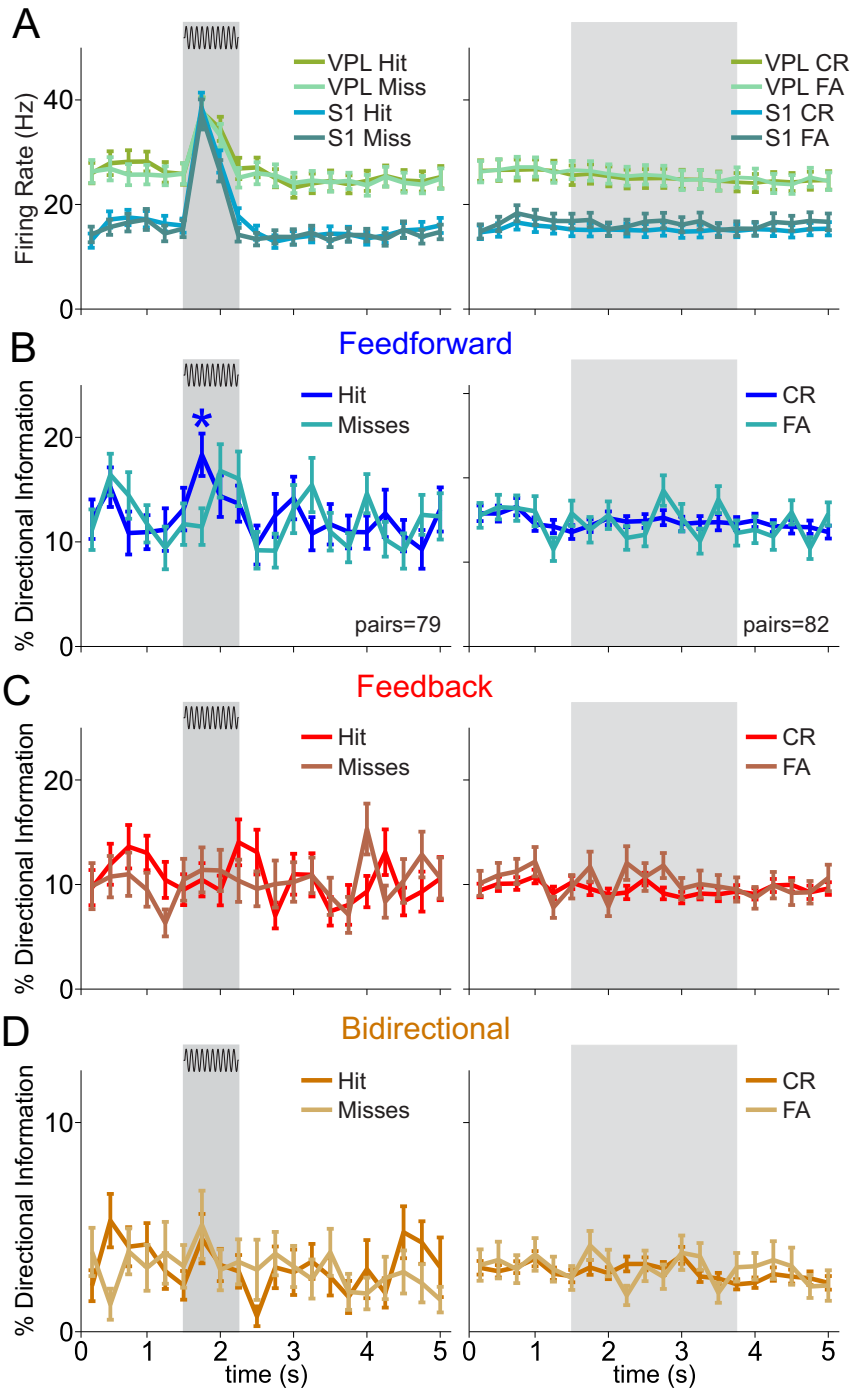

Figure 8. VPL-S1 directional information (DI) during correct and error trials. We analyzed hit and miss trials for threshold amplitudes as well as correct rejection trials and false alarms across all VPL-S1 neuron pairs. (A) Time course of the mean firing rate VPL (n = 48) and S1 (n = 70) neurons during stimulus present trials and for VPL (n=51) and S1 (n=73) neurons during stimulus-absent trials. Neuronal responses were separated according to the monkey's behavioral output. Left panel represents hits and misses for the stimulus-present trials, whereas the right panel represents correct rejections and false alarms for stimulus-absent trials. Neurons and pairs were selected to have more than two trials at near-threshold amplitude for each condition. (B) Time course for the percentage of feedforward information. (C) Time course for the percentage of feedback information. (D) Time course for the percentage of bidirectional information. Left panels in B-D depict hits (dark colors) and misses (light colors) for the stimulus-present trials (neuron pairs = 79; trials = 443 hits; trials = 389 misses). Right panels in B-D depict correct rejections (dark colors) and false alarms (light colors) for the stimulus-absent trials (neuron pairs = 82; trials = 4188 correct rejections; trials = 933 false alarms). Asterisks denote significance levels (*, $P<0.05$) associated with effect sizes (Cohen's H) larger than 0.2.

Supplementary Information Text

Methods

Detection task

Stimuli were delivered to the skin of the distal segment of one digit of the restrained hand, via a computer-controlled stimulator (BME Systems, MD; 2-mm round tip). The initial probe indentation was 500 μm. Vibrotactile stimuli consisted of trains of 20 Hz mechanical sinusoids (20 ms duration each sinusoid), with amplitudes of 1-34 μm (Fig. 1A). These were interleaved with an equal number of trials where no mechanical vibrations were delivered to the skin (amplitude = 0). A trial began when the probe tip (PD) indented the skin of one fingertip of the restrained, right hand, upon which the monkey placed its free, left hand on an immovable key (KD). After a variable pre-stimulus period (1.5-3 s), a vibrotactile stimulus could be presented or not (0.5 s). After a fixed delay period (3 s), the stimulator probe was lifted off from the skin (PU), indicating to the monkey that it could initiate the response movement (KU) to one of two buttons (PB). The button pressed indicated whether or not the monkey felt the stimulus (henceforth referred as 'yes' and 'no' responses, respectively). They were rewarded with a drop of liquid for correct responses. Psychometric detection curves were obtained by plotting the proportion of 'yes' responses as a function of the stimulus amplitude (left panel of Fig. 1B). Depending on whether the stimulus was present or absent and on the behavioral response, the trial outcome was classified as hit, miss, false alarm or correct rejection (right pane of Fig. IB). Monkeys were handled according to the institutional standards of the National Institutes of Health and Society for Neuroscience. All protocols were approved by the Institutional Animal Care and Use Committee of the Instituto de Fisiología Celular of the National Autonomous University of Mexico (UNAM).

In addition to the experimental condition described above, the animals also performed a passive control task (referred as passive condition) during which the stimulus was present or absent, but no response was required (1). Monkeys were

rewarded randomly during the occurrence of the passive condition. Under this situation, sensory information enters or not to the somatosensory system, but no decision and perceptual report is required to obtain a reward.

Recordings

Neuronal recordings were obtained by using two arrays, each with seven independent, movable microelectrodes (2 −3 MΩ; [2, 3]). One array was inserted into S1 (cyan spot on the figurine of left panel of Fig. 1C), in the cutaneous representation of the fingers (areas 1 or 3b; middle panel of Fig. 1C). The other array was located lateral and posterior to the hand's representation (green spot on the figurine of left panel of Fig. 1C) in a way that allowed us to lower the microelectrodes to the cutaneous representation of the fingers in the VPL of the somatosensory thalamus (right panel of Fig. 1C). Recordings were performed contralateral to the stimulated hand (right) and ipsilateral to the responding hand (left). Each recording began with a mapping session to find the cutaneous representation of the fingers in VPL. Subsequently, we mapped neurons in S1 sharing receptive fields with the neurons of VPL (Fig. 1D). All recorded neurons had small cutaneous receptive fields with quickly (QA, VPL n = 65, S1 n=71) or slowly adapting (SA, VPL n = 9, S1 n=4) properties. Locations of the electrode penetrations in VPL and S1 were confirmed with standard histological techniques. The neuronal signal of each microelectrode was sampled at 30 kHz and spikes were sorted online. A more extensive description of the task and recording procedure can be found in previous publications (1, 3).

Here, we report data from multiple recording sessions during which spikes were obtained. For the experimental condition, we recorded 47 sessions with 120−140 trials per session (53 neurons in VPL, 75 neurons in S1, 84 VPL-S1 pairs). For the passive control condition, we obtained 21 sessions with 70-140 trials (21 neurons in VPL, 36 neurons in S1). We performed a fully balanced comparative analysis between the original and control task recordings to mitigate confounding effects. To do so, we only considered VPL-S1 neuron pairs that were recorded in both

experimental conditions. In addition, for each of these pairs, we performed trial subsampling to obtain the same type and number of amplitude classes recorded in the vibrotactile detection and the passive stimulation task. As a result, the pairing pre-processing yielded 36 VPL-S1 pairs that were recorded in both conditions: 1307 stimulus-present trials and 1364 stimulus-absent trials that could be used for unbiased statistical comparison (Fig. 6). In the comparative analysis, we removed the first two intervals of both tasks due to the presence of signal artifacts in the passive condition. Hence, this analysis was restricted to the sub-period $0.5 - 5$s in both tasks (Fig. 6).

Single-trial *DI* estimation: Pre-processing, quantification and significance testing.

We used custom-built MATLAB codes to analyze the data. The directionality analysis presented here is a refinement of our previous method to analyze spike-train directional correlations (4). We estimated directional information between every neuron pair within a population using a Bayesian estimator of the directed information-theoretic measure (5) between a pair of discrete time series that were assumed to be generated according to a Markovian process. In more specific terms, for a pair time series (x^T, y^T) of length T, where $x^T = (x_1, \dots, x_T)$ and $y^T = (y_1, \dots, y_T)$, a time delay $D \geq 0$, and Markovian orders equal to $M_1 > 0$ and $M_2 > 0$, respectively, the directed information-theoretic measure between the underlying stationary processes of x^T and y^T, i.e., (X, Y), is estimated through the formula:

$$\hat{I}_D(X \to Y) \triangleq \frac{1}{T}\sum_{t=1}^{T}\sum_{y_t}\hat{P}\left(Y_t = y_t \middle| X_{t-D-M_2}^{t-D} = x_{t-D-M_2}^{t-D}, Y_{t-M_1}^{t-1} = y_{t-M_1}^{t-1}\right) * log\frac{\hat{P}\left(Y_t=y_t \middle| X_{t-D-M_2}^{t-D}=x_{t-D-M_2}^{t-D}, Y_{t-M_1}^{t-1}=y_{t-M_1}^{t-1}\right)}{\hat{P}\left(Y_t=y_t \middle| Y_{t-M_1}^{t-1}=y_{t-M_1}^{t-1}\right)},$$

[Eq. S1]

where, the joint and marginal probability distributions of (X, Y) are estimated using the context-tree weighting algorithm (CTW, [6, 7]). Matlab code for the CTW-based

estimation of the directed information-theoretic measure can be downloaded from https://web.stanford.edu/~tsachy/DIcode/. Equation 1 quantifies the information that the past of X^T at delay D, i.e., $X_{t-D-M_2}^{t-D}$, has about the present of Y^T, i.e., Y_t, given the most recent part of Y^T, i.e., $Y_{t-M_1}^{t-1}$. This estimator is consistent as long as the two neuronal time series (X^T, Y^T) form a jointly stationary irreducible aperiodic finite-alphabet Markov process whose order does not exceed the prescribed maximum depth in the CTW algorithm (6). Prior to estimating the directed information-theoretic measure, we preprocessed our data as follows. For a single trial, we first binarized spike-train trials using bins of 1ms (mapping 1 to each bin with at least one spike and 0, otherwise). Second, in stimulus-present trials, we removed the variable-time pre-stimulus period in every trial and aligned all trials to the stimulus onset time. In contrast, in stimulus-absent trials, we aligned the trials to the probe down event (PD). We then divided each trial time series into twenty non-overlapping task intervals of 0.25s (250 bins). At each task interval, the spike train was assumed to be generated by a random process that satisfied the estimator requirements with a maximum memory of 2ms ($M_1 = M_2 = 2$ bins) both for the joint and the marginal spike-train processes. Under the estimator requirements, it can be easily checked that the directed information-theoretic measure is asymptotically equivalent to the transfer entropy measure (8) in the limit of the time-series length. To assess that neurons were able to express minimal information through their spike-train responses, we assessed the significance of the entropy value (a particular case of the directed information-theoretic measure when X^T and Y^T coincide) of each spike train at every task interval with maximum memory, $M = 2$. This step removed segments of spike trains with zero or small number of spikes. Finally, among those pairs of spike-train segments with significant entropy, we ran the delayed directed information-theoretic measure estimator (Eq. S1) at time delays D=0, 2, 4, 6, 8, 10, 12, 14, 16, 18, 20 ms.

We dealt with the multiple test problem over delays by using the maximum directed information-theoretic measure over all preselected delays as a test statistic:

$$I_{\mathrm{STAT}}(X \to Y) \triangleq \max_{D\epsilon[0,2,\cdots,20]} \hat{I}_D\,(X \to Y) \qquad \text{[Eq. S2]}$$

To assess the significance of the above statistic (Eq. S2), we used a Monte-Carlo permutation test (9). In this test, the original (i.e., non-permuted) estimation was compared with the tail of a distribution obtained by performing 20 equally-spaced (to maximize independent sampling) circular shifts of the target spike train Y^T within the range [50,200]ms and computed the corresponding P-value (10). Hence, the significance test provides three outputs: the significance assessment $(0/1)$, the statistic value and the maximizing delay $\widehat{D}$. In particular, any spike-train pair during a trial is considered to convey directional information (*DI*) at a given task interval if the corresponding test yields significance.

Statistical analysis: Quantification of significant effects on *DI* percentages

The main metric used in Figs. 3-7 was obtained by aggregating each *DI* type (feedforward, feedback and bidirectional) over all neuron pairs and trials at individual task intervals and computing their percentage over the total amount of trials. In Fig. 8, however, the percentage was computed over trials per neuron pair and then percentages were averaged over neuron pairs.

Therefore, the main results illustrated in Figs. 3-8 were obtained by comparing *DI* percentages under usually two conditions. Comparisons of this metric were of two types: paired and unpaired. Paired comparisons appeared in the comparison between the VPL→S1 and VPL→S1 percentages (Fig. S1), the percentages over neuron pairs in different conditions (Fig. S3), the percentages between the original and control task (Fig. 6) and the percentages over neuron pairs for correct and error trials (Fig. 8). Unpaired comparisons appeared when assessing the stimulus-driven change in the percentage of directional information (Figs. 3A, 7A). In paired or unpaired comparisons of *DI* percentages we frequently used non-parametric tests for correlated samples (11) using statistics based on Cohen's effect size (Cohen's *h*; [12]) that measured the distance between proportions. The use of this statistic allows to straightforwardly quantify the size of any significant effect by comparing

its value with standarized thresholds (*H = 0.2*, small effect size; *H = 0.5*, medium effect size; *H = 0.8* large effect size), thus avoiding sample size biases. For any unpaired comparison between proportion p_1 and p_2, we used the original Cohen's *h* measure:

$$H^{\text{unpaired}}(p_1, p_2) = 2\left(\arcsin\sqrt{p_1} - \arcsin\sqrt{p_2}\right) \quad \text{[Eq. S3]}$$

For paired comparison, we proposed the following paired version of Cohen' *h*:

$$H^{\text{paired}}(p_1, p_2) = \text{sign}(\bar{p}) * 2\arcsin\sqrt{|\bar{p}|} \quad \text{[Eq. S4]}$$

where $\bar{p} = \frac{p_1 - p_2}{2}$.

Non-parametric tests for correlated samples were performed through 1000 group-based permutations (11) where groups were defined to be either single trials (Figs. 3-7) or neuron pairs (Fig. 8) and group sample sizes were maintained in each permutation. Thus, our analysis avoided introducing any statistical bias to the sampled reference distribution. Most statistical comparisons were independently performed over task intervals (*N = 20*). To correct for interval multiplicity (e.g. Fig. S1), we applied the Holm-Bonferroni procedure (13), which provided a significance threshold that controlled the Familywise Error Rate (FWER) at a significance level (α *= 0.05*). In the remaining tests performed at different amplitude values or neuron pairs, multiplicity was not corrected for lack of sufficiently large sample sizes.

In Fig. 6B we applied single-trial and average-trial correlation measures to quantify the non-parametric correlation (Spearman's rank-order correlation) between *DI* percentages and stimulus amplitudes. Single-trial correlation values were obtained by correlating the trial-based binary vector associated to each *DI* type against their corresponding amplitudes. Average-trial correlations were obtained by first computing the overall percentage of *DI* at each amplitude and then by correlating these percentages against all amplitude values.

Statistical analysis: Influence of neuronal firing rates into *DI* percentages

A great deal of the results was devoted to assess the influence of the firing rates of driver and target neurons into the *DI* measured in our data set (Figs. S4, S7A and B, 4 and 7). In particular, we made of use of Spearman's correlation to correlate the firing rate of simultaneous neuronal spike trains in VPL and S1 with the existence of *DI* $(0/1)$ between them across all trials. More precisely, we independently correlated the trial-based binary vector associated to the *DI* against the firing rate in VPL and S1 spike trains, respectively. We performed this computation in general for the *DI* against driver and target firing rates (Figs. S4A and S4B), and in particular for each *DI* type, feedforward, feedback and bidirectional, against VPL and S1 firing rates in every task interval (Figs. S4C and S4D and Figs. S7A and S7B). Moreover, we compared the firing rates of neurons in VPL and S1 holding the distinct *DI* types (Figs. 4, 7B and C). These later comparisons are intrinsically unpaired (in trials) as the amount of *DI* trials may differ across types. Hence, we made use of Wilcoxon rank-sum test to assess statistical differences in *DI*-dependent firing rates.

Statistical analysis: Contribution of zero-lag and non-zero lag to bidirectional information

By definition (See section "Single-trial *DI* estimation" above), each *DI* is associated to a (maximizing) delay. Hence, to study the contribution of individual time delays to each *DI* type we started by plotting their histograms in Fig. S2B using aggregated data from task intervals within or outside the stimulus period and the PWS. These histograms pinpointed the great percentage of bidirectional information at time delay 0 ms, especially during the stimulus-presence. We therefore examined in Fig. 7 and S7 the contribution of 0 ms delays to the main results reported for bidirectional information. To do so, we divided all bidirectional information estimates into two disjoint groups: one bidirectional group where the *DI* across each direction was estimated at 0 ms delay, and a second group where both were estimated at a delay different from 0 ms. The formed group is referred

in the main text as zero-lag bidirectional information, whereas the second group is referred to as non-zero lag bidirectional information. We then considered these groups as *DI* sub-types and performed on them the main analysis of the study in Fig. 7 and Fig. S7. Specifically, we repeated those analyses leading to Fig. 3A (Fig. 7A), Fig. 4 (Fig. 7B and 7C), Fig. S4 (Fig. S7A and S7B), Fig. 5 (Fig. S7C) and Fig. 6 (Fig. 7D).

Simulation study

In Fig. S5, we made use of two stochastic models (Unidirectional and Bidirectional) to simulate pairs of spike trains from two different neurons eliciting firing rates within the range of our dataset and assess the sensitivity of our *DI* estimation method and the correlation between the *DI* and the firing rate induced by the estimation method. The simulation of spike-train pairs was randomly and independently generated on a trial-by-trial basis according to two paradigms: a unidirectional model, which is associated to the reported feedforward and feedback information, and a bidirectional model, which is associated to bidirectional information. Under each paradigm, single-trial spike trains were modeled as binary sequences generated via conditional probabilities relying on *signal* (δ, λ) and *noise* parameters (ε, ν). The range of these parameters was chosen to fit the range of neuronal firing rates found during the first half (250ms) of the stimulus period during hit trials. Each model was used to test the sensitivity of the *DI* estimation against the firing rate of either the target, driver or both simultaneous recorded neurons (Fig. S5C and S5D). In particular, we used the bidirectional model to test whether the *DI* sensitivity was significantly different between zero-lag and non-zero lag bidirectional information. In addition, each model served to test the correlation of the *DI* with the firing rate. To obtain a fair comparison with the correlation values observed in the real data, each model was mixed with realizations of independent spike train pairs so that the simulated data mimicked the overall *DI* percentage observables while still approximating the average firing rates in driver and target neurons (Fig. S5E and S5F). Then, the correlation values were shown as a function of increasing *DI* percentages (Fig. S5G and S5H), which corresponded to increasing weights of each paradigm in the mixed model. Further details can be found in Fig. S5.

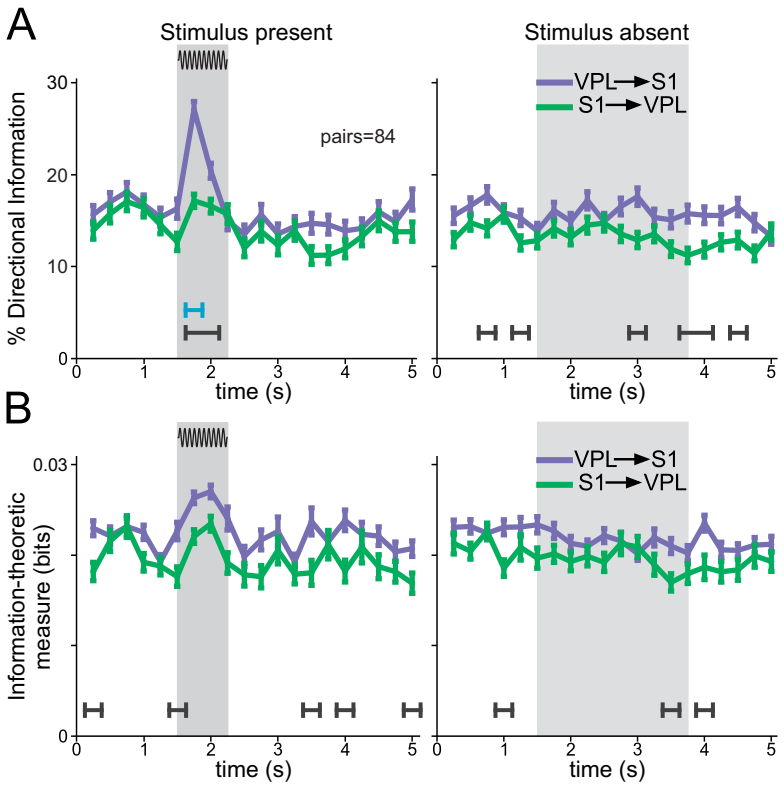

Fig. S1. VPL→S1 and S1→VPL directional information (*DI*) during the detection task. Time course of the task for the percentage of directional information (*DI*) and the average (unbiased) information-theoretic measure estimate over *DI* pairs between VPL→S1 (purple) and S1→VPL (green) in stimulus-present (left panel, trials = 3216 hit; neuron pairs = 84) and stimulus-absent trials (right panel, trials = 4371 correct rejections; neuron pairs = 84). Only paired trials where at least one spike train attained a minimal firing rate of 35Hz were selected for the computation. In all figures, grey boxes depict the stimulation period for the stimulus-present trials, and the possible window of stimulation (PWS) for the stimulus-absent trials). Error bars denote the SEM (standard error of the mean). (A) Percentage of *DI*. Black lines depict intervals for which the difference between *DI* was significantly different ($P < 0.05$; non-parametric test, multiple-test corrected; effect size > 0.3). Blue lines depict significant intervals for which the effect size was larger than 0.5. (B) Time course of information-theoretic measure for VPL→ S1 (purple) and S1→ VPL (green) directional information. Black lines depict intervals for which the difference between directions was significantly different ($P < 0.05$; non-parametric test, multiple-test corrected; effect size > 0.3). Here and in the next time-varying figures, we removed the variable-time pre-stimulus period in every stimulus-present trial and aligned all trials to the stimulus onset. In stimulus-absent trials, we aligned the trials to the probe down event (PD).

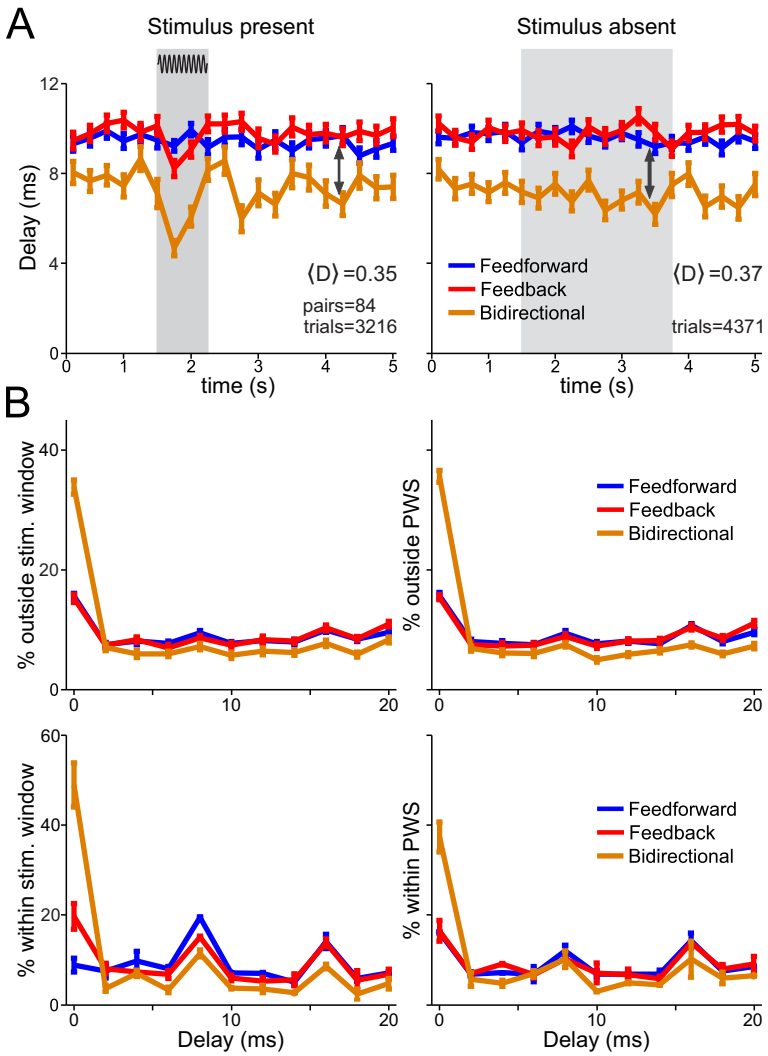

Fig. S2. Mean delay for feedforward, feedback and bidirectional information. Related to Fig. 3 (A) Time course of the task for the mean delays occurring during feedforward, feedback and bidirectional information for stimulus present (left, trials=3216 hits; neuron pairs = 84) and stimulus absent (right, trials=4371 correct rejections; neuron pairs = 84) trials. ⟨D⟩ Indicates the average value of the Cohen's D effect size (over task intervals and *DI t*ypes) between joint feedforward and feedback, and bidirectional information. (B) Percentage of delays outside (upper panel) or within (lower panel) the stimulation or possible window of stimulation (PWS) for stimulus present (left) and stimulus absent (right) trials, respectively. Error bars denote the SEM (standard error of the mean).

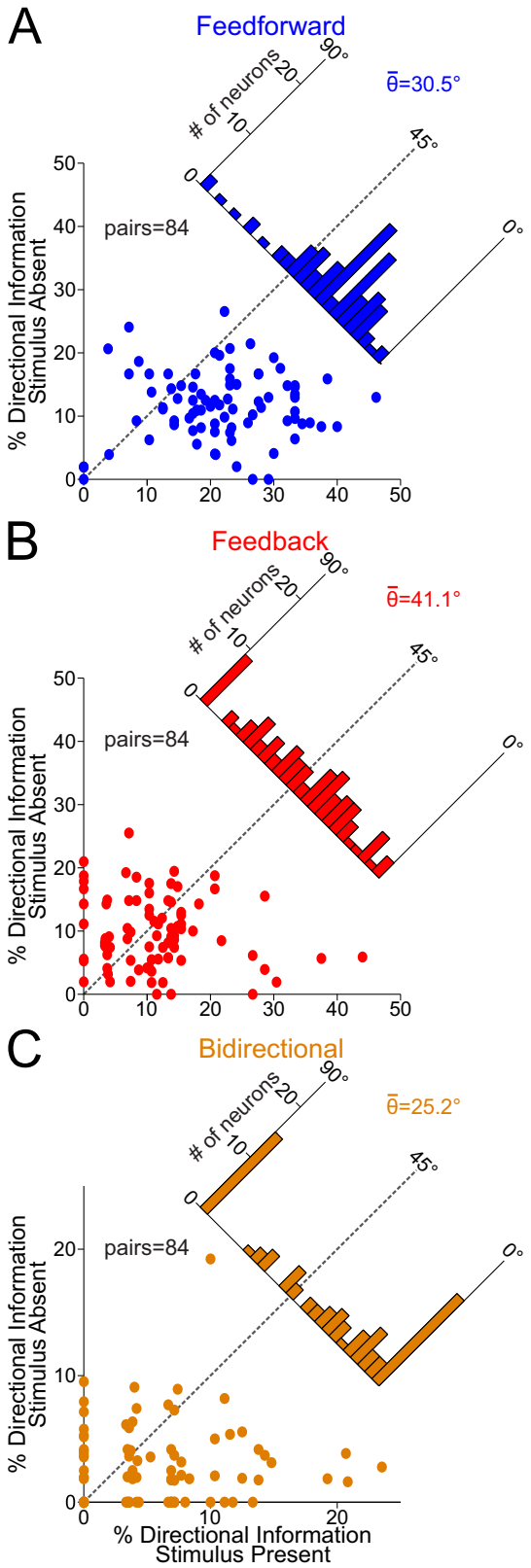

Fig. S3. Directional Information (*DI*) comparison between stimulus-present and stimulus-absent trials. Related to Fig. 3. Percentage of (A) feedforward, (B) feedback, and (C) bidirectional information per neuron pair (trials = 3216 hits; trials = 4371 correct rejections; neuron pairs = 84) during the first interval (0-0.25s) of the stimulus period in stimulus-present trials vs. the first interval (0-0.25s) of the possible window of stimulation (PWS) in stimulus-absent trials. In each panel the insets depict the histograms of the angular deviation between stimulus-absent and stimulus-present trials over all neuronal pairs and indicates its median. The percentage for all three types of *DI* was higher during the stimulus-present trials ($\theta < 45°$) with feedforward ($\theta = 30.5°$) and bidirectional ($\theta = 25.2°$) information exhibiting larger differences across conditions than feedback ($\theta = 41.1°$) information.

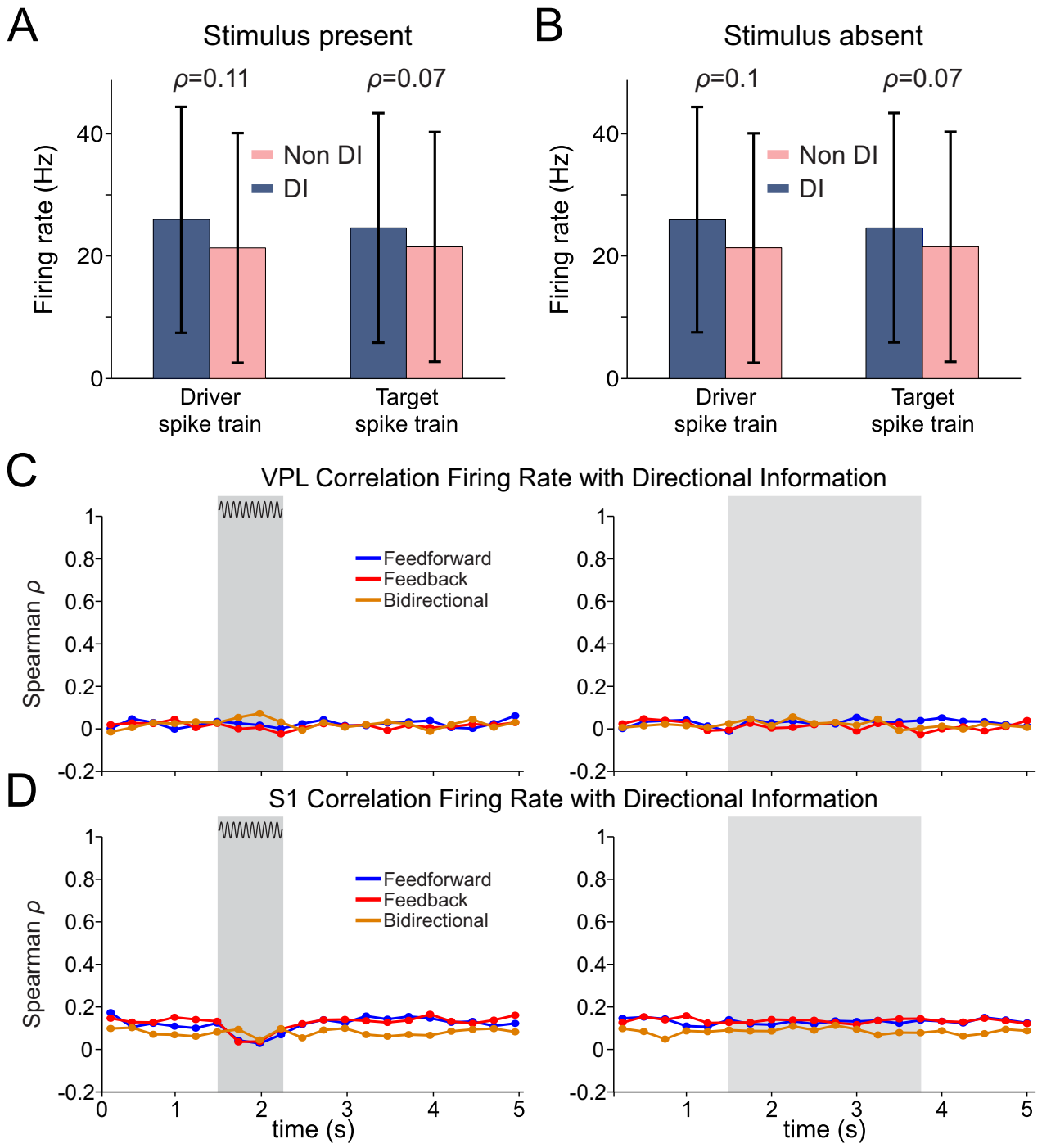

Fig. S4. Correlation between firing rate and directional information (*DI*) types. Related to Fig. 3 and 4. Mean firing rate for driver and target neurons holding *DI* and non *DI* across the VPL→S1 and S1→VPL neuron pairs (84). (A) Mean firing rate and standard deviation for driver and target neurons for the stimulus-present trials. Blue depicts firing rates related to *DI* (*DI* intervals = 29074; trials = 3216 hits). Pink depicts firing rates related to non *DI* (non-*DI* intervals = 177286). The value of ρ indicates the Spearman correlation value obtained from correlating the firing rate of the driver/target with the existence of incoming/outgoing *DI*. (B) Same as in (A) but for the stimulus-absent trials (*DI* intervals = 28253; non-*DI* intervals = 178027; trials = 4371 correct rejections). (C) Spearman's correlation between the firing rate in VPL neurons and the existence of feedforward, feedback or bidirectional information with a S1 neuron during the time course of the task during stimulus-present (left; trials = 3216 hits) and stimulus-absent (right; trials = 4371 correct rejections) trials. (D) Similar as panel C, but for S1 neurons holding *DI* with VPL neurons.

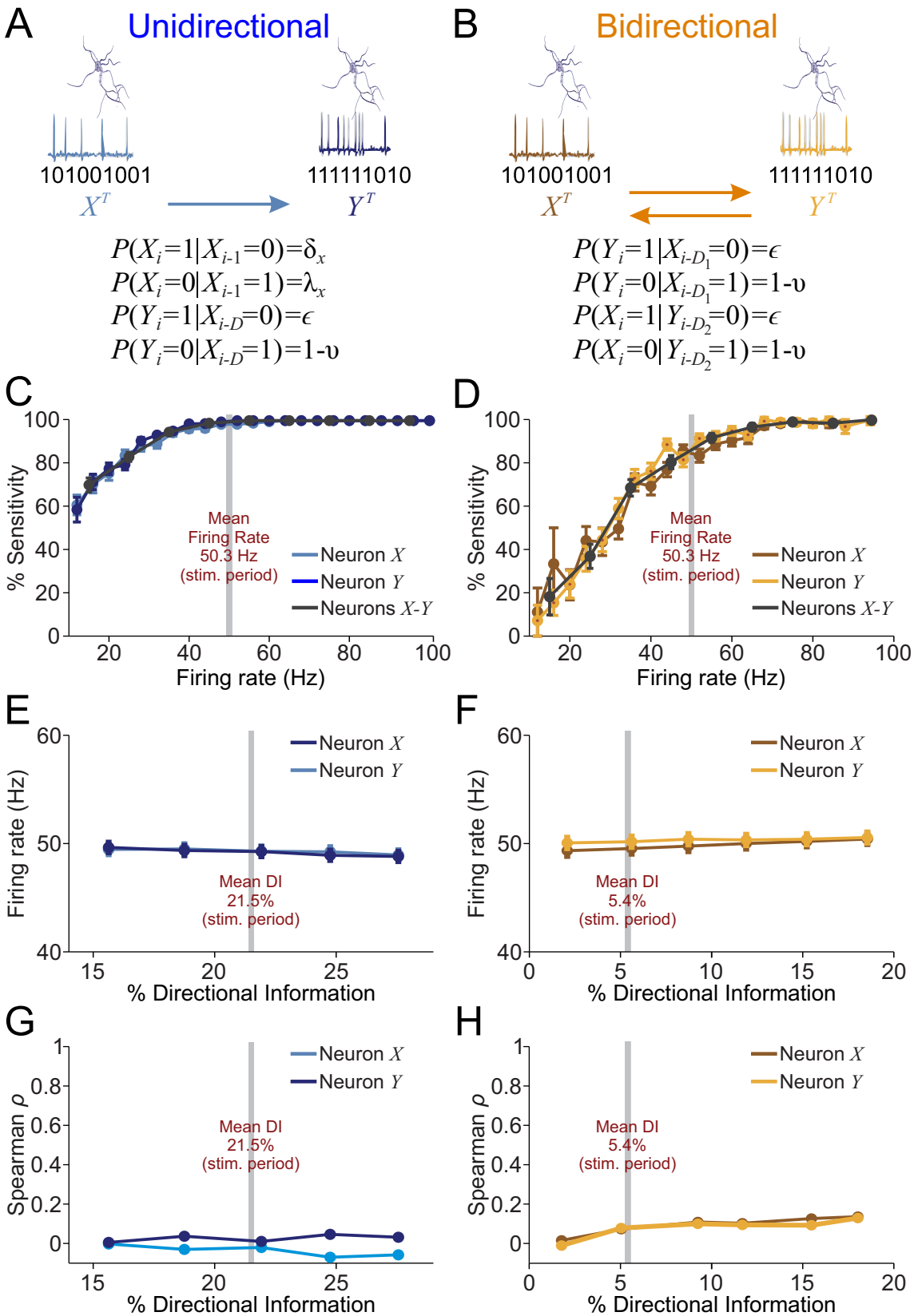

Fig. S5. Unidirectional and Bidirectional simulation models. Related to Fig. 3 and 4. We simulated pairs of spike trains (N=3850 trials) from two different neurons eliciting firing rates within the range of our data set to assess (1) the sensitivity of our *DI* estimation method and (2) the correlation between the *DI* and the firing rate induced by the estimation method. Pairs of spike trains were randomly and independently generated according to two simulation paradigms: unidirectional model, which is associated to the reported feedforward and feedback information, and bidirectional model, which is associated to bidirectional information. Under each paradigm, single-trial spike trains were modeled as T-length binary sequences ($X_T=[X_1,...,X_T]$ and $Y_T=[Y_1,...,Y_T]$), which were generated by probabilistic models with parameters chosen to fit the range of neuronal firing rates found during the first half (250ms) of the stimulus period during hit trials. (A) Unidirectional model: The single-trial spike train of the driver neuron is denoted as X^T and is modeled as a binary Markov chain of order 1 with two autocorrelation parameters (δ_x, λ_x), which characterize the *neuronal*

signal, i.e., the spiking probability of X^T after a silent bin, $\delta_X = P(X_i=1 | X_{i-1}=0)$ and the spiking probability of X_T after a spike, $\lambda_X = P(X_i=1 | X_{i-1}=1)$. On the other hand, the single-trial spike train of the target neuron is denoted as Y^T and is characterized by a transformation of the process X^T that depends on 3 parameters (D, ε, v). D stands for the delay at which the coupling between both spike trains occurs while ε and v parametrize the *channel noise*, i.e., the spiking probability of Y^T after a silent bin, $\varepsilon = P(Y_i=1 | X_{i-D}=0)$, and the spiking probability of Y^T after a spike bin in X^T, $v = P(Y_i=1 | X_{i-D}=1)$. (B) Bidirectional model. The bidirectional coupling between X^T and Y^T is modeled by 4 parameters (D_1, D_2, ε, v). D_1 and D_2 stand for the delays in each direction at which the coupling occurs, respectively, while ε and v parametrize in an unbiased form the noise across both unidirectional links, $X_T \rightarrow Y_T$ and $Y_T \rightarrow X_T$. (C)-(D) Sensitivity percentage of the *DI* estimation for both simulation models. Gray line in each panel depicts the mean neuronal firing rate in real-data recordings during the first half of the stimulus period during hit trials (50,33Hz). Curves that are function of joint target and driver neurons are constructed by binning firing rates from both neurons in consecutive 10Hz bins (10-20Hz, 20-30Hz, etc.) and plotting the sensitivity values at bin midpoints. Error bars denote the SEM (standard error of the mean) across simulation realizations. (C) Sensitivity percentage of the *DI* estimation method in the unidirectional model as a function of firing rate of the driver (X^T), target (Y^T) and both neurons. In total, an ensemble of spike train pairs (simulated trials=3850) were uniformly generated with T=250 bins across autocorrelation parameters δ_X=0.02:0.01:0.08 and λ_X=0.05, and noise parameters ε=0.013 and v=0.35:0.1:0.45. Delays were uniformly drawn over D=0:2:20 bins. Error bars denote the SEM (standard error of the mean). (D) Sensitivity percentage of the *DI* estimation method in the bidirectional model as a function of firing rate of the driver (X^T), target (Y^T) and both neurons. In total, spike train pairs (simulated trials=1925) were uniformly generated with T=250 bins across noise parameters ε=0.013 and v=0.35:0.1:0.45 and delays uniformly drawn over D_1, D_2 =0:2:20 bins. Error bars denote the SEM (standard error of the mean). In this model the difference between the sensitivity of zero-lag and non-zero lag bidirectional information was not found significant (Wilcoxon rank-sum test, P>0.05, SI Appendix). (E)-(H) To fit the *DI* estimation percentages found in real data recordings, both models were mixed with an ensemble of independently generated spike train pairs (simulated trials =3850 for unidirectional model; simulated trials =1925 for bidirectional model) with autocorrelation parameters δ_X=0.02:0.01:0.08 and λ_X=0.05. To sample different *DI* percentages, the mixing factor α varied from α=0 (all pairs belong to the independent ensemble) to α=1 (all pairs belong to the uni/bidirectional model) in steps of 0.04 keeping always the total number of trials equal. In each panel, the gray line depicts the overall *DI* percentage for either unidirectional (21.5%) or bidirectional information (5.4%). Error bars denote the SEM (standard error of the mean) across simulation realizations. (E) Average firing rate of driver (X^T) and target neurons (Y^T) in the mixed unidirectional model as a function of the *DI* percentage. (F) Same as Panel (E) but for the mixed bidirectional model. (G) Correlation between *DI* and the driver (X^T) and target neurons (Y^T) firing rate in the mixed unidirectional model as a function of the *DI* percentage. (H) Same as panel E, but for the mixed bidirectional model.

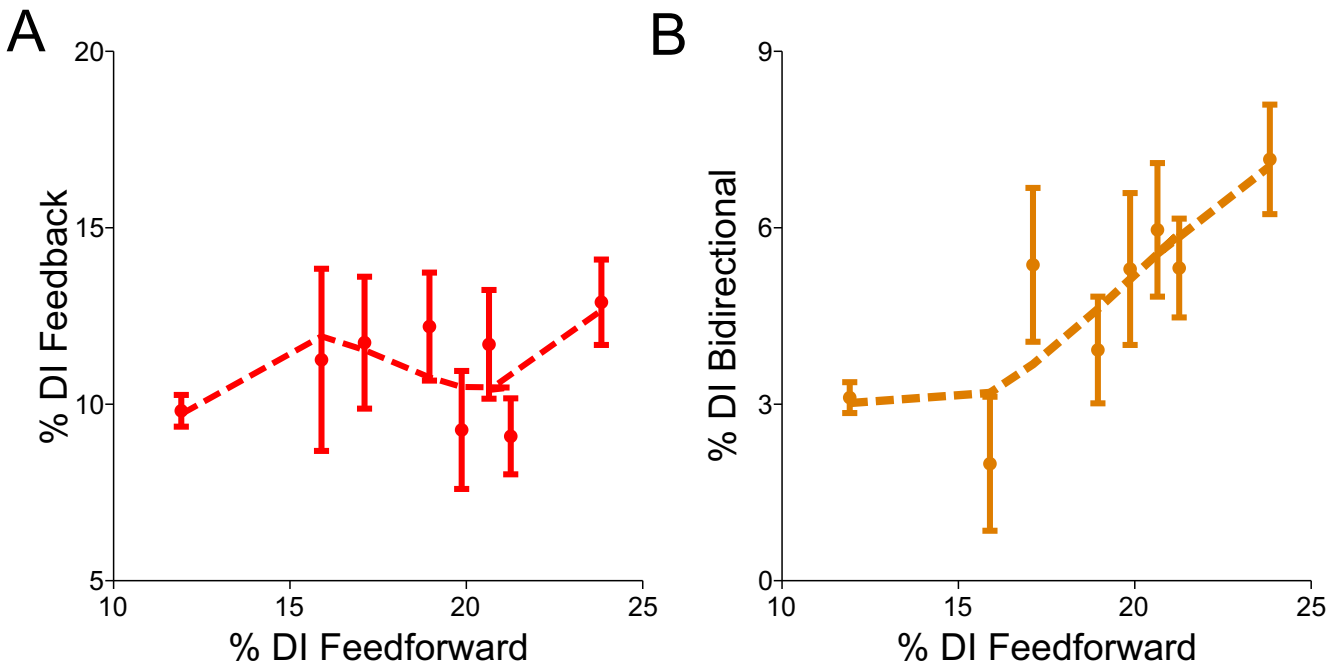

Fig. S6. Relationship of the amount of feedback and bidirectional information with respect to feedforward information across distinct stimulus amplitudes. Related to Fig. 5 (A) Relationship between %*DI* feedback and %*DI* feedforward for all stimulus amplitude values analyzed in the study. (B) Relationship between %*DI* bidirectional and %*DI* feedforward for all stimulus amplitude values analyzed in the study. Error bars denote the standard error of the mean (SEM).

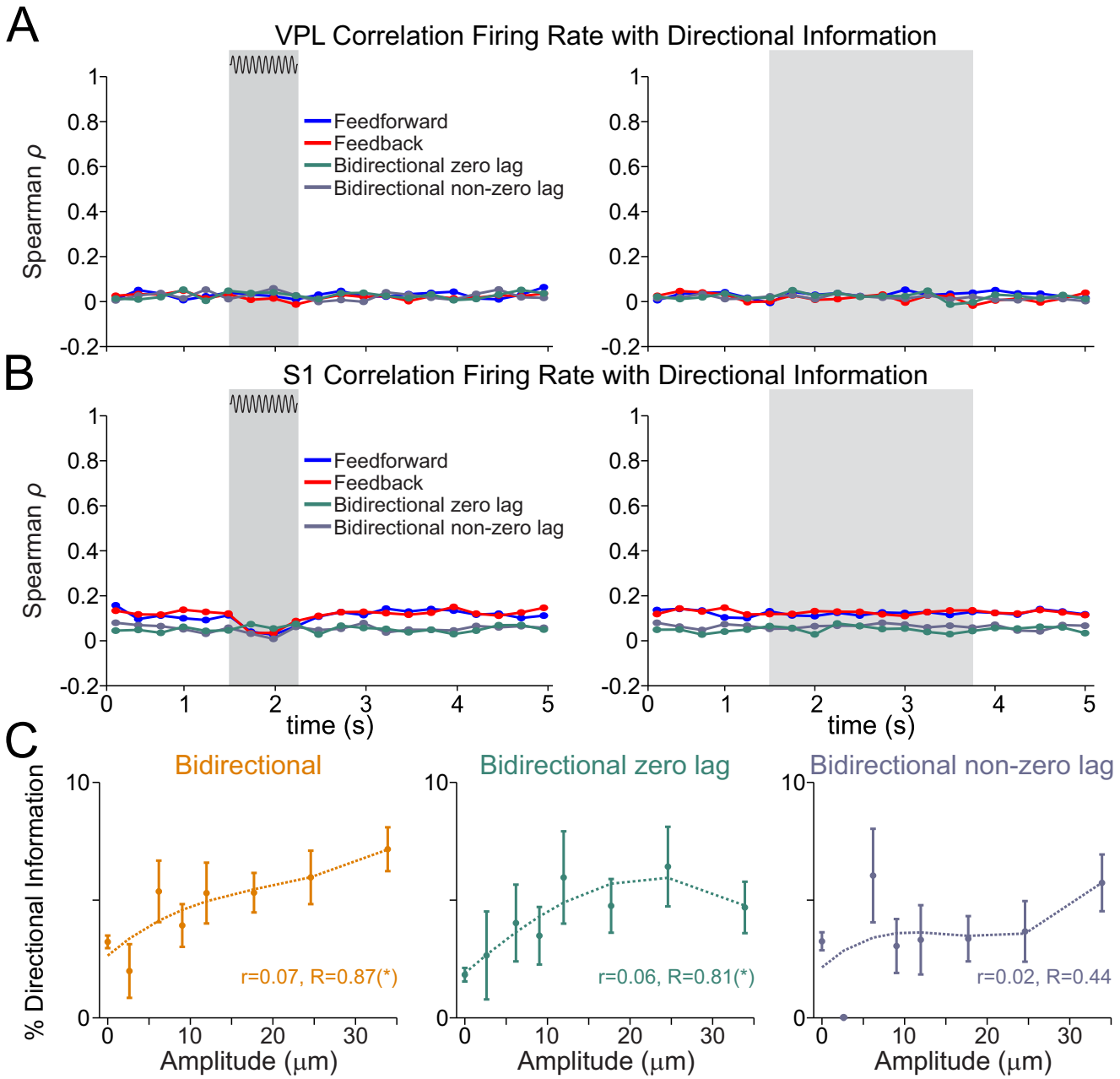

Fig. S7. Influence of neuronal firing rate and stimulus amplitudes on zero-lag and non-zero lag bidirectional information. Related to Fig. 8 (A) Spearman's correlation between the firing rate in VPL neurons and the existence of overall and either zero-lag or non-zero lag bidirectional information, respectively, with a S1 neuron during the time course of the task during stimulus-present (left; trials = 3216 hits) and stimulus-absent (right; trials = 4371 correct rejections (B) Same as panel A, but for neurons in S1 holding bidirectional information with VPL neurons. (C) Mean percentage of overall (left), zero-lag (middle) and non-zero lag (right) bidirectional information as a function of the stimulus amplitude during the first half of the stimulation period (left, 0 − 0.25 s). The value of *r* is the correlation between the stimulus amplitude and the existence of *DI* in each type across all trials (no amplitude-averages) with Spearman correlation (trials = 7587). The value R is the analogous correlation considering amplitude-average values (amplitudes = 8). Asterisks depict significance (*, $P < 0.05$; Spearman correlation). Error bars denote the SEM (standard error of the mean).

References

1. Vázquez Y, Zainos A, Alvarez M, Salinas E, Romo R (2012) Neural coding and perceptual detection in the primate somatosensory thalamus. *Proc Natl Acad Sci USA* 109:15006–15011.
2. Romo R, Brody CD, Hernández A, Lemus L (1999) Neuronal correlates of parametric working memory in the prefrontal cortex. *Nature* 399:470–473.
3. Hernández A, Nácher V, Luna R, Alvarez M, Zainos A, Cordero S, Camarillo L, Vázquez Y, Lemus L, and Romo R (2008) Procedure for recording the simultaneous activity of single neurons distributed across cortical areas during sensory discrimination. *Proc Natl Acad Sci USA* 105: 16785-16790.
4. Tauste Campo A, Martinez-Garcia M, Nácher V, Luna R, Romo R, Deco G (2015) Task-driven intra- and interarea communications in primate cerebral cortex. *Proc Natl Acad Sci USA* 112:4761–4766.
5. Massey J. (1990). Causality, feedback and directed information. *In Proc Int Symp Inf Theory Applic* 27–30.
6. Jiao J, Permuter HH, Zhao L, Kim YH, Weissman T (2013) Universal estimation of directed information. *IEEE Trans Inf Theory* 59(10):6220–6242.
7. Willems FM, Shtarkov YM, Tjalkens TJ (1995) The context-tree weighting method: basic properties. *IEEE Trans. Inf. Theory* 41(3):653-664.
8. Schreiber T (2000) Measuring Information Transfer. *Phys Rev Lett* 85:461-464.
9. Ernst MD (2004) Permutation Methods: A Basis for Exact Inference. *Stat Sci* 19:676–685.
10. Phipson B, Smyth GK (2010) Permutation P-values should never be zero: calculating exact P-values when permutations are randomly drawn. *Stat Appl Genet Mol Biol*, 9(1).
11. Winkler AM, Ridgway GR, Webster MA, Smith SM, Nichols TE (2014) Permutation inference for the general linear model. *Neuroimage* 92:381-397.

12. Cohen J (1988) Statistical power analysis for the behavioral sciences. Hillsdale, NJ: Academic Press
13. Holm S (1979) A Simple Sequentially Rejective Multiple Test Procedure. *Scand J Stat* 6:65–70.